Cell Reports
Article

ATM Regulates Adipocyte Differentiation and Contributes to Glucose Homeostasis

Masatoshi Takagi,[1,10,*] Hatsume Uno,[1,2,10] Rina Nishi,[1] Masataka Sugimoto,[3] Setsuko Hasegawa,[1] Jinhua Piao,[1] Norimasa Ihara,[4] Sayaka Kanai,[5] Saori Kakei,[6] Yoshifumi Tamura,[6] Takayoshi Suganami,[7] Yasutomi Kamei,[8] Toshiaki Shimizu,[9] Akio Yasuda,[3] Yoshihiro Ogawa,[5] and Shuki Mizutani[1]

[1]Department of Pediatrics and Developmental Biology, Graduate School of Medicine, Tokyo Medical and Dental University, 1-5-45 Yushima, Bunkyo-ku, Tokyo 113-8519, Japan
[2]Medical Business Unit, Sony Corporation, 1-5-45 Yushima, Bunkyo-ku, Tokyo 113-8519, Japan
[3]Section of Biochemistry, National Institute for Longevity Sciences, NCGG, 36-3 Gengo, Moriokacho, Obu, Aichi 474-8522, Japan
[4]Department of Reproductive Biology, National Research Institute for Child Health and Development, 2-10-1 Ohkura, Setagaya-ku, Tokyo 157-0074, Japan
[5]Department of Molecular Endocrinology and Metabolism, Graduate School of Medicine, Tokyo Medical and Dental University, Japan Science and Technology Agency, CREST, 1-5-45 Yushima, Bunkyo-ku, Tokyo 113-8519, Japan
[6]Department of Medicine, Metabolism & Endocrinology, Juntendo University, School of Medicine, 2-1-1 Hongo, Bunkyo-ku, Tokyo, 113-0033, Japan
[7]Department of Organ Network and Metabolism, Graduate School of Medical and Dental Sciences, Tokyo Medical and Dental University, Japan Science and Technology Agency, PRESTO, 1-5-45 Yushima, Bunkyo-ku, Tokyo 113-8519, Japan
[8]Laboratory of Molecular Nutrition, Graduate School of Environmental and Life Science, Kyoto Prefectural University, Hangicho 1-5, Shimogamo, Kyotoshi, Kyoto 606-8522, Japan
[9]Department of Pediatrics and Adolescent Medicine, Juntendo University, School of Medicine, 2-1-1 Hongo, Bunkyo-ku, Tokyo 113-0033, Japan
[10]Co-first author
*Correspondence: m.takagi.ped@tmd.ac.jp
http://dx.doi.org/10.1016/j.celrep.2015.01.027

SUMMARY

Ataxia-telangiectasia (A-T) patients occasionally develop diabetes mellitus. However, only limited attempts have been made to gain insight into the molecular mechanism of diabetes mellitus development in A-T patients. We found that $Atm^{-/-}$ mice were insulin resistant and possessed less subcutaneous adipose tissue as well as a lower level of serum adiponectin than $Atm^{+/+}$ mice. Furthermore, in vitro studies revealed impaired adipocyte differentiation in $Atm^{-/-}$ cells caused by the lack of induction of C/EBPα and PPARγ, crucial transcription factors involved in adipocyte differentiation. Interestingly, ATM was activated by stimuli that induced differentiation, and the binding of ATM to C/EBPβ and p300 was involved in the transcriptional regulation of C/EBPα and adipocyte differentiation. Thus, our study sheds light on the poorly understood role of ATM in the pathogenesis of glucose intolerance in A-T patients and provides insight into the role of ATM in glucose metabolism.

INTRODUCTION

Ataxia-telangiectasia (A-T) is often accompanied by glucose intolerance and insulin resistance (Bar et al., 1978; Blevins and Gebhart, 1996; McFarlin et al., 1972; Morio et al., 2009; Schalch et al., 1970), and our previous study revealed that 17% of A-T patients developed type 2 diabetes mellitus (Morio et al., 2009). A-T patients also exhibit poor weight gain, a progressive decrease in their BMI, and progressive dystrophy (Schubert et al., 2005). In addition to A-T patients, A-T carriers, who comprise an estimated 0.05%–0.1% of the normal population, suffer an increased risk of ischemic heart disease (Su and Swift, 2000) and diabetes (Morrell et al., 1986). As in A-T patients, glucose intolerance has been reported in $Atm^{-/-}$, $Atm^{+/-}ApoE^{-/-}$, and $Atm^{-/-}ApoE^{-/-}$ mice (Miles et al., 2007; Schneider et al., 2006); the $Atm^{+/-}ApoE^{-/-}$ mouse model generates a state of insulin resistance similar to that observed in type 2 diabetes. In addition, Miles et al. reported impaired insulin secretion in aged $Atm^{-/-}$ mice (Miles et al., 2007). However, the mechanism by which an ATM deficiency affects the development of type 2 diabetes remains unknown.

ATM, the gene responsible for A-T, plays a central role in the DNA damage response. Previous reports have suggested that ATM is activated in response to insulin stimulation and phosphorylates the Cap-dependent translation inhibitor 4E-BP1 (Yang and Kastan, 2000). A recent large-scale proteomic ATM substrate analysis identified several proteins involved in the insulin-signaling pathway, such as AKT and FOXO1 (Matsuoka et al., 2007). Together, these observations strongly support the hypothesis that ATM is involved in the insulin-signaling pathway and modulates glucose homeostasis.

Insulin resistance is a frequent complication of obesity; however, lipoatrophic diabetes is paradoxical because it is

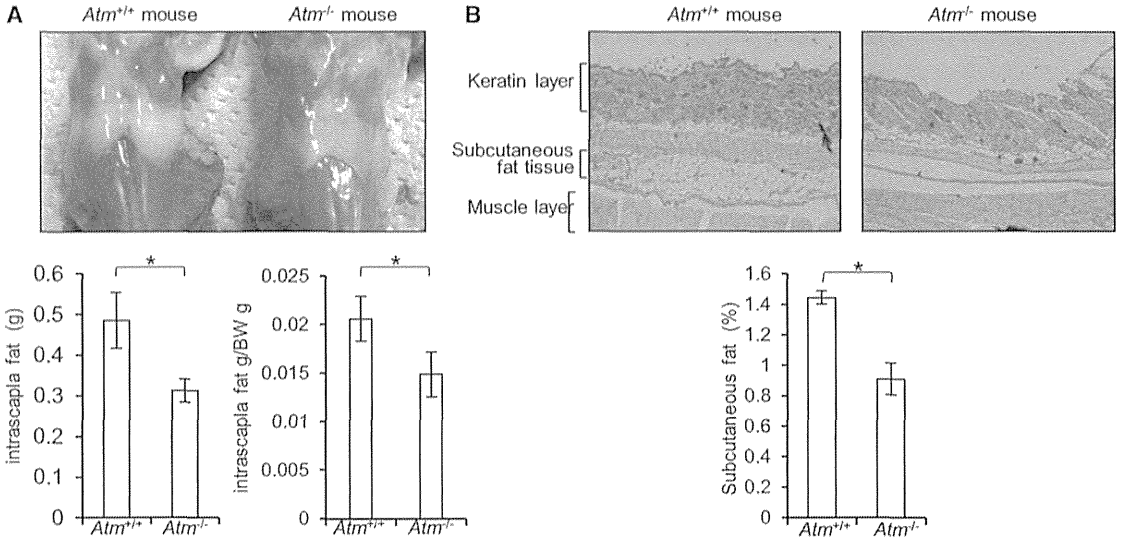

Figure 1. Adipose Tissue Distribution in *Atm*$^{+/+}$ and *Atm*$^{-/-}$ Mice

(A) Intrascapular fat tissue and (B) hematoxylin-eosin staining of the back skin of *Atm*$^{+/+}$ and *Atm*$^{-/-}$ mice. The lower graphs indicate the amount of fat tissue. The *Atm*$^{-/-}$ mice were relatively smaller than the *Atm*$^{+/+}$ mice. The relative amount of fat tissue per body weight is also shown. The mean values from three independent experiments are shown (A and B).

characterized by insulin resistance despite the existence of a low-fat mass. Insulin resistance in lipoatrophic diabetes may be due to the defective development of adipose tissue and the subsequently impaired secretion of adipokines, such as adiponectin or leptin (Rosen and Spiegelman, 2006). Adipocytes secrete several adipokines, such as adiponectin, leptin, visfatin, and omentin, which increase insulin sensitivity. Conversely, adipokines that are secreted by hypertrophic adipocytes, such as resistin and tumor necrosis factor α (TNF-α), act to decrease insulin sensitivity. Alterations in adiposity have profound implications for glucose homeostasis, and an appropriate balance of adiposity is required to maintain adequate glucose homeostasis.

The central engine for adipose differentiation involves CCAAT/enhancer-binding protein α (C/EBPα) and peroxisome proliferator activated receptor γ (PPARγ). When this receptor is activated by an agonistic ligand in fibroblasts, a full program of differentiation is stimulated, including morphological changes, lipid accumulation, and the expression of almost all genes characteristic of fat cells. Multiple C/EBPs, such as C/EBPβ and C/EBPδ, are expressed during the early stages of differentiation; subsequently, C/EBPα and PPARγ expression is driven by C/EBPβ and C/EBPδ. C/EBPs and PPARγ also directly activate many genes in terminally differentiated adipocytes (Rosen and Spiegelman, 2000).

To understand the molecular mechanism of diabetes development in A-T patients, we investigated the adipose tissue distribution and degree of adipocyte maturation in *Atm* knockout mice. Examination of mouse embryonic fibroblasts (MEFs) derived from wild-type (*Atm*$^{+/+}$) or *Atm* knockout (*Atm*$^{-/-}$) mice revealed that adipocytic differentiation did not occur in *Atm*$^{-/-}$ MEFs. The impaired adipocyte differentiation observed in *Atm*$^{-/-}$ MEFs was due to the defective ATM-dependent induction of C/EBPα and PPARγ expression. These observations strongly support the hypothesis that glucose intolerance and insulin resistance in A-T patients are due to attenuated adipocyte functioning.

RESULTS

Atm Knockout Mice Exhibited Glucose Intolerance, Insulin Resistance, and Abnormal Adipose Distribution

As previously suggested, *Atm*$^{-/-}$ mice were glucose intolerant, and their condition mimicked type 2 diabetes mellitus (Figures S1A–S1G). Interestingly, *Atm*$^{+/-}$ mice exhibited neither glucose intolerance nor insulin resistance, although *Atm*$^{+/-}$ male mice fed a high-fat diet exhibited glucose intolerance and insulin resistance (Figures S1H and S1I). A-T patients have lean figures and a reduced level of subcutaneous fat tissue. In contrast, an increased amount of visceral fat tissue was reported in *Atm*$^{+/-}$*ApoE*$^{-/-}$ mice (Schneider et al., 2006). Therefore, the adipose distribution in *Atm*$^{-/-}$ mice was re-evaluated. We detected a decreased amount of intrascapular and subcutaneous fat tissue in *Atm*$^{-/-}$ mice compared to their wild-type littermates (Figures 1A and 1B). Conversely, *Atm*$^{-/-}$ mice showed an increased level of visceral fat tissue, as previously reported, similarly to human metabolic syndrome, which is also associated with a high accumulation of visceral fat (Matsuzawa, 2006) (Figures S1J–S1L). In addition, a reduced serum level of adiponectin was previously observed in *Atm*$^{+/-}$*ApoE*$^{-/-}$ mice (Schneider et al., 2006). As expected, *Atm*$^{-/-}$ mice also showed reduced serum adiponectin and leptin levels, whereas *Atm*$^{+/-}$ mice exhibited levels intermediate between those of *Atm*$^{-/-}$ and *Atm*$^{+/+}$ mice (Figures S1M and S1N). The fat redistribution, increase in visceral fat tissue, and reduction in subcutaneous fat tissue observed in *Atm*$^{-/-}$ mice may be explained by their increased appetite, which is due to their reduced level of leptin (Figure S1O).

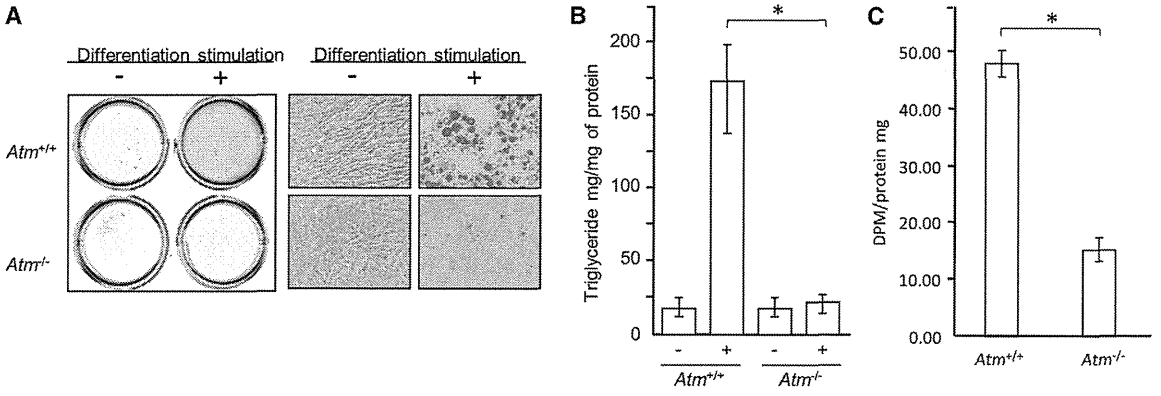

Figure 2. ATM-Null Cells Are Defective in Adipocyte Differentiation

(A) Oil red O staining of in-vitro-differentiated $Atm^{+/+}$ and $Atm^{-/-}$ MEFs. The right panel shows magnified images of parts of the left panel.

(B) The intracellular triglyceride concentrations of $Atm^{+/+}$ and $Atm^{-/-}$ MEFs are shown.

(C) In-vitro-differentiated $Atm^{+/+}$ and $Atm^{-/-}$ MEFs were assayed for radiolabeled 2-deoxyglucose uptake in the presence of 5 μg/ml insulin.

The SEs are shown as error bars (*$p < 0.05$).

ATM-Deficient Cells Were Defective in Adipocyte Differentiation

The reduced amount of subcutaneous fat tissue and reduced level of serum adiponectin in *Atm* knockout mice suggested a defect in adipocyte functioning. To evaluate the function of adipose tissue in *Atm* knockout mice, an in vitro adipocyte differentiation model (Tanaka et al., 1997) was employed, using $Atm^{-/-}$ and $Atm^{+/+}$ MEFs. After the MEFs were stimulated to differentiate into adipocytes, the $Atm^{+/+}$ MEFs showed lipid accumulations, as indicated by Oil red O staining, whereas the $Atm^{-/-}$ MEFs failed to differentiate into adipocytes (Figure 2A). To evaluate the ability of the cells to differentiate into adipocytes, the intracellular triglyceride levels of these cells after differentiation stimulation were compared. $Atm^{-/-}$ MEFs showed an approximately 85% triglyceride level compared with that of $Atm^{+/+}$ MEFs (Figure 2B). Glucose uptake was evaluated in cells that were induced to differentiate for 6 days, and the $Atm^{-/-}$ MEFs showed approximately 75% less glucose uptake compared to $Atm^{+/+}$ MEFs (Figure 2C). Adipocyte differentiation capacity using stromal vascular fractions (SVFs) from $Atm^{+/+}$ and $Atm^{-/-}$ mice was also examined. As observed in the MEFs, the $Atm^{-/-}$ SVFs exhibited a defective adipocyte differentiation capacity (Figure S2A).

Adipocyte differentiation experiments frequently utilize 3T3-L1 preadipocytes. To confirm the results obtained using $Atm^{-/-}$ and $Atm^{+/+}$ MEFs and SVFs, adipocyte differentiation was also investigated in 3T3-L1 cells treated with the ATM inhibitors caffeine and KU55933. As expected, treatment with caffeine and KU55933 blocked adipocyte differentiation in 3T3-L1 cells (Figure S2B). To confirm that adipocytic differentiation was dependent on ATM function, the genome of $Atm^{-/-}$ MEFs was complemented with wild-type or kinase-dead ATM cDNA via expression vectors; only wild-type ATM restored the in vitro ability of the cells to differentiate into adipocytes (Figure S2C). ATM-deficient cells accumulate reactive oxygen species (ROS) (Ito et al., 2004), which may interfere with differentiation in vitro. To investigate whether ROS interfered with adipocyte differentiation, $Atm^{-/-}$ MEFs were pretreated with the ROS scavenger N-acetyl cysteine (NAC), and differentiation was induced in the presence of NAC. However, NAC treatment failed to rescue adipocyte differentiation in $Atm^{-/-}$ MEFs (Figure S2D). These experiments demonstrated that ATM is required for proper adipocyte differentiation and that ROS are not involved in this process.

ATM-Deficient Cells Showed Defective Induction of Transcriptional Factors Required for Adipocyte Differentiation

To clarify the molecular mechanism of attenuated adipocyte differentiation in $Atm^{-/-}$ MEFs, several factors with possible roles in adipocyte differentiation were investigated in $Atm^{+/+}$ and $Atm^{-/-}$ MEFs upon differentiation induction. C/EBPα and PPARγ expression was observed 4–6 days after the induction of differentiation in $Atm^{+/+}$ MEFs, whereas $Atm^{-/-}$ MEFs completely lacked C/EBPα and PPARγ expression. In contrast, C/EBPβ and C/EBPδ expression was induced normally upon the differentiation of $Atm^{-/-}$ MEFs (Figure 3A). A-T cells have been previously reported to show decreased expression of the IGF1 receptor, which is the primary mediator of the insulin-signaling pathway (Peretz et al., 2001; Shahrabani-Gargir et al., 2004). However, there was no significant difference in the levels of expression of the IGF1 receptor of $Atm^{+/+}$ and $Atm^{-/-}$ MEFs (Figure 3A). These two observations suggested that signaling pathways upstream of C/EBPβ and C/EBPδ were regulated normally in $Atm^{-/-}$ MEFs during differentiation and that the impaired adipocyte differentiation of $Atm^{-/-}$ MEFs was caused by defective C/EBPα and PPARγ expression. Real-time qPCR and northern blot revealed that the expression of C/EBPα and PPARγ mRNA was dysregulated at the transcriptional level (Figures 3B, 3C, and S2E). KU55933 blocked adipocyte differentiation in 3T3-L1 cells (Figure S2B), which was accompanied by the aberrant induction of C/EBPα expression (Figure S2F). Adipocyte differentiation via wild-type ATM complementation of $Atm^{-/-}$ MEFs restored the induction of C/EBPα expression, whereas kinase-dead ATM complementation failed to restore this process (Figure S2G).

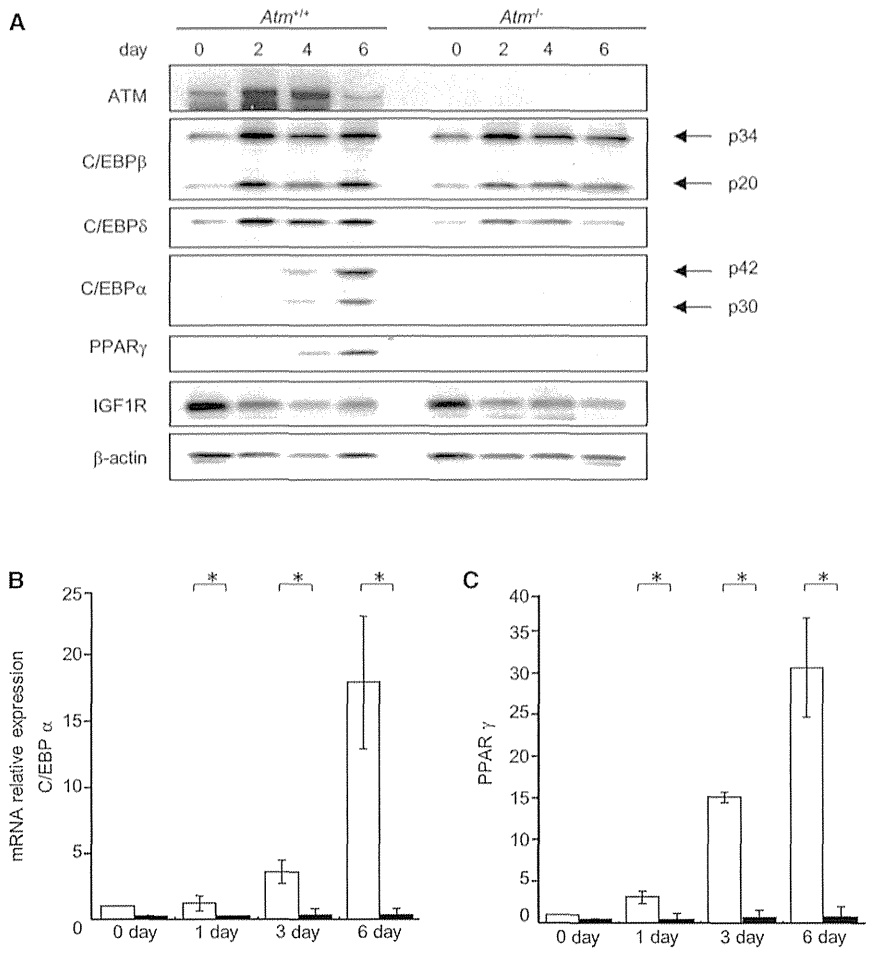

Figure 3. C/EBPα and PPARγ Expression during the Adipocyte Differentiation Process

(A) Western blotting analyses of in-vitro-differentiated $Atm^{+/+}$ and $Atm^{-/-}$ MEFs.

(B and C) The levels of C/EBPα and PPARγ mRNA expression after differentiation were analyzed with qRT-PCR. The mean values from three independent experiments are shown in the bar graphs. The SEs are shown as error bars (*$p < 0.05$).

These results suggested that the impaired adipocyte differentiation observed in $Atm^{-/-}$ cells was caused by a defect in the ATM-dependent transcriptional activation of C/EBPα and PPARγ expression upon differentiation stimulation.

Complementation of C/EBPα or PPARγ Restored the Adipocyte Differentiation Capacity of $Atm^{-/-}$ Cells

C/EBPα and PPARγ are necessary for the terminal differentiation of adipocytes, and the aberrant expression of C/EBPα and PPARγ is thought to be the central cause of impaired adipocyte differentiation in $Atm^{-/-}$ MEFs. Thus, we tested whether defective differentiation would be rescued by the overexpression of C/EBPα or PPARγ in $Atm^{-/-}$ MEFs. $Atm^{-/-}$ MEFs were transduced using retroviruses for the expression of HA-tagged C/EBPα or FLAG-tagged PPARγ2 and the internal ribosome entry sequence (IRES)-dependent expression of GFP, and then GFP-positive cells were cultured under conditions that stimulated differentiation. The overexpression of either HA-tagged C/EBPα or FLAG-tagged PPARγ2 restored the ability of $Atm^{-/-}$ MEFs to differentiate into adipocytes (Figures S2H and S2J). Furthermore, the overexpression of HA-tagged C/EBPα or FLAG-tagged PPARγ2 induced the endogenous expression of PPARγ or C/EBPα (Figures S2I and S2K).

ATM-Deficient Cells Were Deficient in Cell-Cycle Regulation after Differentiation Stimulation

In addition to the major adipocyte transcriptional differentiation inducers, such as C/EBPα or PPARγ, several factors that participate in cell-cycle regulation are involved in adipocyte differentiation (Abella et al., 2005; Fajas et al., 2002). Upon differentiation stimulation, the cells that are arrested by contact inhibition re-enter the cell cycle, in a process referred to as clonal expansion (Tang et al., 2003). After two to three rounds of proliferation, the cell cycle is halted in these cells, and they enter the process of terminal differentiation (Rosen and Spiegelman, 2000). Thus, the cell-cycle kinetics of $Atm^{+/+}$ and $Atm^{-/-}$ MEFs undergoing differentiation was investigated. The results of a bromodeoxyuridine (BrdU) pulse-labeling experiment revealed that $Atm^{+/+}$ and $Atm^{-/-}$ MEFs re-entered the cell cycle normally after differentiation stimulation, but the cell cycle was not halted in $Atm^{-/-}$ MEFs at 8 days after differentiation stimulation (Figure S3A). Monitoring the RB phosphorylation status using western blotting analysis showed lack of RB dephosphorylation at the terminal stage of differentiation in $Atm^{-/-}$ MEFs (Figure S3B). The induction of cyclin A expression upon differentiation stimulation was also observed in $Atm^{+/+}$ and $Atm^{-/-}$ MEFs; cyclin A expression declined at 6 days after differentiation stimulation in $Atm^{+/+}$ MEFs, but its expression persisted in $Atm^{-/-}$ MEFs (Figure S3C). The expression of E2F4, which halts the adipogenic differentiation process (Fajas et al., 2002), was gradually upregulated, reaching a maximum level at 6 days after differentiation stimulation in $Atm^{+/+}$ MEFs. Interestingly, the level of expression of E2F4 was constitutively high in $Atm^{-/-}$ MEFs (Figure S3C). These observations demonstrated that, although $Atm^{-/-}$ MEFs could re-enter the clonal expansion phase, they failed to show the cell-cycle arrest necessary for the terminal differentiation process. Interestingly, the overexpression of HA-tagged C/EBPα induced cell-cycle arrest after the clonal expansion of $Atm^{-/-}$ MEFs via RB dephosphorylation (Figures S3D and S3E), suggesting that C/EBPα functions upstream of cell-cycle regulators.

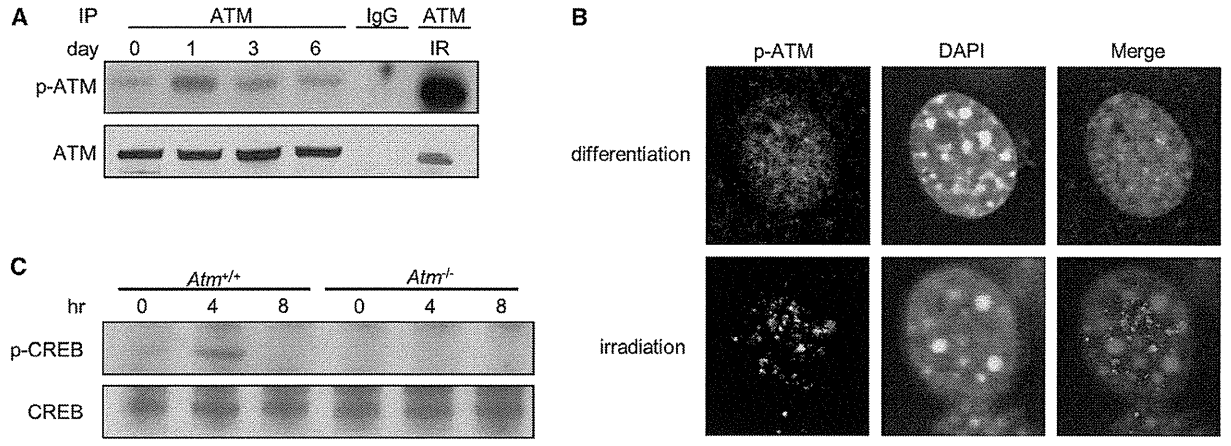

Figure 4. ATM Is Activated during Differentiation

(A) The ATM phosphorylation status after in vitro differentiation was determined by western blotting analysis of immunoprecipitates.

(B) ATM phosphorylation 1 day after in vitro differentiation and 3 hr after 5-Gy irradiation, as detected using immunofluorescence.

(C) CREB phosphorylation upon in vitro differentiation was analyzed using western blotting.

ATM Was Activated by Stimuli that Induce Differentiation

ATM is activated by DNA damage signals as well as insulin stimulation (Yang and Kastan, 2000), and ATM activation can be monitored according to the intermolecular autophosphorylation of its serine-1981 (Bakkenist and Kastan, 2003). Therefore, the autophosphorylation of ATM during adipogenesis was investigated. During adipocyte differentiation, ATM was activated (Figure 4A). Differentiation-stimulated cells showed a diffuse phosphorylated ATM pattern in contrast to the irradiated positive control cells, which showed diffuse and discrete foci of phosphorylated ATM (Figures 4B and S4A). This ATM activation process was not associated with DNA double-strand breakage (Figure S4B). ATM activation upon differentiation stimulation also resulted in the phosphorylation of the ATM downstream target CREB at serine-121 (Shi et al., 2004), which is required for adipocyte differentiation (Zhang et al., 2004) (Figure 4C).

ATM Was Required for the Induction of C/EBPα Transcription by C/EBPβ

The above-described results strongly suggest that ATM activation contributes to adipogenesis via the regulation of C/EBPα and/or PPARγ transcription, although the expression of C/EBPβ and C/EBPδ was induced normally in $Atm^{-/-}$ MEFs. C/EBPβ and C/EBPδ are involved in C/EBPα transcription through binding to the C/EBP-binding sequence in the C/EBPα promoter and acting as upstream transcription factors for C/EBPα. Therefore, C/EBPβ binding to the C/EBPα promoter was investigated. Chromatin immunoprecipitation (ChIP) assays revealed that C/EBPβ bound equally to the C/EBPα promoter in $Atm^{+/+}$ and $Atm^{-/-}$ MEFs upon differentiation stimulation (Figure 5A). However, the activity of the C/EBPα promoter, as determined using a luciferase assay, was completely abolished in $Atm^{-/-}$ MEFs (Figure 5B). Furthermore, this dysregulation of C/EBPα transcription attenuated the histone H3 and H4 acetylation in the C/EBPα promoter region (Figure 5C). Together, these experiments showed that C/EBPβ bound to the C/EBPα promoter but could not transactivate the C/EBPα promoter in the absence of ATM.

ATM Bound to C/EBPβ and p300 Was Recruited to the ATM-C/EBPβ Complex

An electromobility shift assay (EMSA) revealed a protein complex bound to the C/EBPα promoter in $Atm^{+/+}$ and $Atm^{-/-}$ MEFs. However, examination of nuclear extracts of $Atm^{-/-}$ MEFs showed that the mobility of several protein complexes that bind to the C/EBPα promoter was retarded in these cells (Figure S5), suggesting that the composition or modification of protein complexes that bind to the C/EBPα promoter were different in $Atm^{+/+}$ and $Atm^{-/-}$ MEFs. The C/EBPβ binding partners in $Atm^{+/+}$ and $Atm^{-/-}$ MEFs were investigated using an immunoprecipitation assay, which showed that ATM bound to C/EBPβ upon differentiation stimulation (Figure 6A). C/EBPβ is known to bind to CBP/p300, a phosphorylation target of ATM, and modulate its transcriptional activity (Jang et al., 2010; Schwartz et al., 2003; Wang et al., 2007), and the acetylation of histone H3 and H4 near the C/EBPα promoter was attenuated in $Atm^{-/-}$ MEFs. Thus, we hypothesized that histone acetyl transferase is recruited to the ATM-C/EBPβ complex and acetylates histones near the C/EBPα promoter. Therefore, the association of histone acetyl transferase with C/EBPβ was investigated using an immunoprecipitation assay. Screening for several histone acetyl transferases, including GCN5, p300, CBP, and Tip60, demonstrated that ATM and C/EBPβ bound to p300 upon differentiation and that the binding of ATM to C/EBPβ and p300 was augmented upon differentiation stimulation. Furthermore, co-immunoprecipitation assays revealed that ATM, C/EBPβ, and p300 formed a ternary complex upon differentiation stimulation, with C/EBPβ-p300 binding being dependent upon the presence of ATM (Figure 6A). C/EBPβ threonine 188 (threonine 235 in humans) phosphorylation is required for its transcriptional activation; upon differentiation stimulation, $Atm^{+/+}$ MEFs showed phosphorylation of C/EBPβ at threonine 188, whereas this effect was absent in $Atm^{-/-}$ MEFs (Figure 6B).

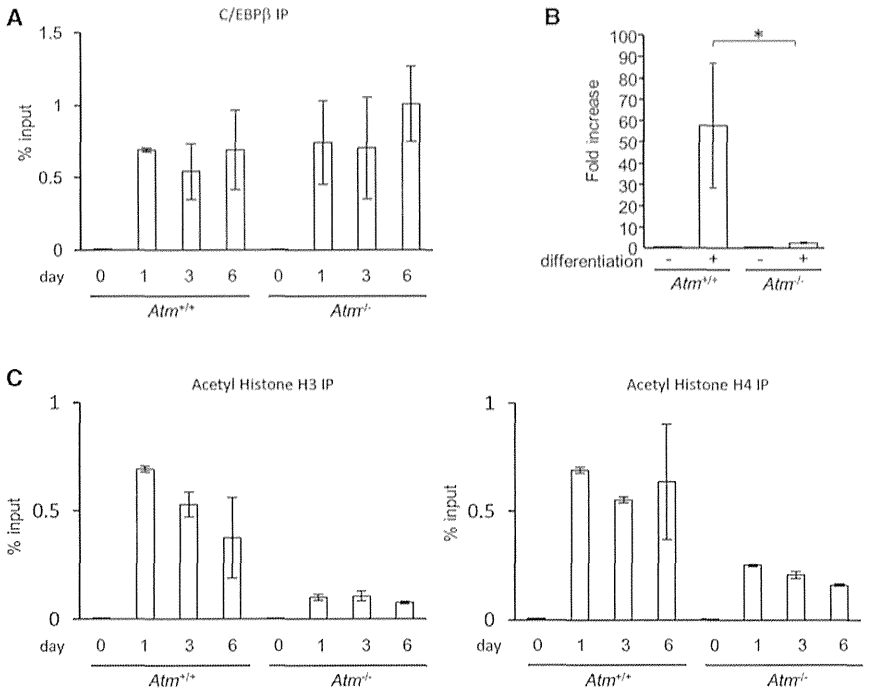

Figure 5. C/EBPβ Transcriptional Activity Depends on ATM

(A) A ChIP assay using an anti-C/EBPβ antibody (H7) showed that C/EBPβ bound to the C/EBPα promoter sequence in $Atm^{+/+}$ and $Atm^{-/-}$ MEFs.

(B) C/EBPα promoter activation in $Atm^{+/+}$ and $Atm^{-/-}$ MEFs before and 3 days after differentiation stimulation, as determined using a luciferase assay.

(C) Analyses of the histone H3 and H4 acetylation status proximal to the C/EBPα promoter using a ChIP assay. The mean values from three independent experiments are shown.

The SEs are shown as error bars (*$p < 0.05$).

It is known that C/EBPβ threonine 188 is directly phosphorylated by ERK, and it is also known that $ATM^{-/-}$ cells exhibit defective MAPK activation (Kim and Wong, 2009; Raman et al., 2007). To link these two observations, we tested whether the activation of the MAPK-signaling pathway was defective in $Atm^{-/-}$ cells after differentiation stimulation. As expected, $Atm^{-/-}$ MEFs exhibited defective MEK1 and ERK activation (Figure S6). Thus, the defect in C/EBPβ phosphorylation in $Atm^{-/-}$ cells may be due to the failure of MAPK-signaling pathway activation.

Restoration of Adipose Functioning in $Atm^{-/-}$ Mice Improved Their Glucose Intolerance

Based on our findings, agents such as the PPARγ ligand thiazolidione, which induces adipocyte differentiation, may be effective candidates for treating glucose intolerance in A-T patients. Indeed, rosiglitazone treatment restored adipocyte differentiation in $Atm^{-/-}$ MEFs (Figures 7A and 7B), and pioglitazone treatment ameliorated glucose intolerance in $Atm^{-/-}$ mice (Figures 7C and 7D) and increased their serum adiponectin concentrations (Figure 7E), suggesting a restoration of fat tissue functioning. Metformin treatment also improved glucose intolerance in these mice (Figures 7C and 7D). The increase in insulin sensitivity with metformin treatment was milder than that with pioglitazone treatment; however, the results were not significantly different. Furthermore, metformin treatment did not affect the serum adiponectin concentration, suggesting that metformin improved the glycemic response through a fat-tissue-independent pathway (Figure 7E). Previously, surgical implantation of normal fat tissue was reported to rescue insulin resistance in lipodystrophic mice (Gavrilova et al., 2000). Therefore, we surgically implanted fat tissue derived from wild-type and *Atm* knockout littermates into $Atm^{-/-}$ mice (Figures S7A and S7B), and only wild-type fat transplantation successfully reversed the glucose intolerance and insulin resistance of $Atm^{-/-}$ mice and increased their levels of serum adiponectin (Figures 7F–7H).

DISCUSSION

A-T patients often exhibit glucose intolerance and insulin resistance and possess less subcutaneous adipose tissue than healthy individuals. Glucose intolerance was reported not only in A-T patients, but also in the *Atm* knockout mouse model (Miles et al., 2007; Schneider et al., 2006). We confirmed that *Atm* knockout mice are insulin resistant and possess less subcutaneous adipose tissue, accompanied by a lower level of serum adiponectin, than their wild-type littermates. Furthermore, in vitro investigations using MEFs revealed that adipocyte differentiation was impaired in $Atm^{-/-}$ cells, which was caused by the lack of induction of C/EBPα and PPARγ, crucial transcription factors involved in adipocyte differentiation. These observations suggest that the glucose intolerance and insulin resistance of A-T patients are due to the improper functioning of their adipose tissue due to the attenuation of adipocyte differentiation.

Recently, a link was established between the DNA damage checkpoint pathway and cellular metabolism. Previous reports have shown that the ATM-p53 pathway participates in glucose metabolism (Armata et al., 2010; Minamino et al., 2009), although the molecular mechanisms involved in this process remain unclear. Our findings demonstrate the importance of the DNA damage checkpoint pathway in the regulation of cellular metabolism and homeostasis in vivo. It is also clear that transcriptional regulation by ATM plays an important role in cellular differentiation. ATM is reportedly required for the retinoic-acid-induced differentiation of SH-SY5Y neuroblastoma cells to neuronal-like cells. Retinoic acid rapidly triggers the activity of ATM kinase, resulting in the ATM-dependent phosphorylation of the transcription factor CREB (Fernandes et al., 2007). In the case of adipocyte differentiation, ATM is also activated by extracellular signals. In our model of adipocyte differentiation, C/EBPα transcription required ternary complex formation by ATM, C/EBPβ, and the histone acetyl transferase p300, which was associated with the phosphorylation of C/EBPβ at threonine 235. The recruitment of p300 to the C/EBPβ complex activated the

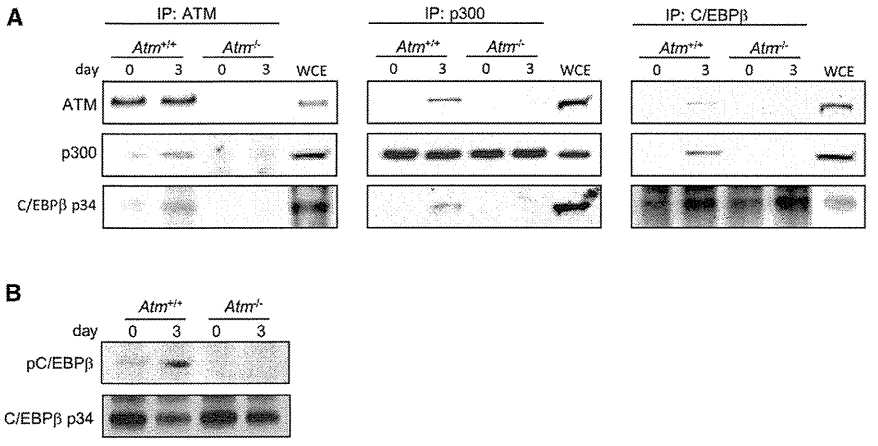

Figure 6. ATM Forms a Ternary Complex with C/EBPβ and p300

(A) ATM bound to p300 and C/EBPβ upon differentiation (left). p300 bound to ATM and C/EBPβ upon differentiation (middle). C/EBPβ bound to ATM and p300 upon differentiation (right). Immunoprecipitation using the indicated antibodies was performed before and after the differentiation of $Atm^{+/+}$ and $Atm^{-/-}$ MEFs. The anti-C/EBPβ (H7) antibody immunoprecipitated only the active p34 LAP form of C/EBPβ.

(B) C/EBPβ was phosphorylated in an ATM-dependent manner. C/EBPβ was immunoprecipitated from $Atm^{+/+}$ and $Atm^{-/-}$ MEF lysates and detected using western blotting with an anti-phospho-C/EBPβ threonine 235 (threonine 188 in mouse) antibody.

C/EBPβ-dependent transcription of C/EBPα through the modification of histone acetylation. The phosphorylation of C/EBPβ at threonine 235, reportedly by ERK and GSK3, is required for its transcriptional activity (Park et al., 2004). Moreover, ERK activation by DNA damage is dependent upon ATM (Tang et al., 2002).

It is possible that other components of the C/EBPβ complex(es) are targets of ATM phosphorylation and that this phosphorylation is a prerequisite for the formation of the complex(es). In fact, C/EBPβ and the C/EBPβ-binding partners p300, CREB, and FOXO1, as well as the negative regulator of adipocyte differentiation Sp1 and the positive regulator of adipocyte differentiation E2F1, carry ATM phosphorylation consensus residues and are phosphorylated by ATM (Iwahori et al., 2008; Jang et al., 2010; Lin et al., 2001). Therefore, the phosphorylation of transcription factors and associated proteins by ATM, including the C/EBPβ-p300 complex, may play a central role in adipocytic differentiation.

The DNA damage response pathway has been linked with the state of cellular glucose metabolism (Armata et al., 2010; Minamino et al., 2009) and fat metabolism (Wong et al., 2009). Furthermore, components of the DNA break/repair machinery, including DNA-PK, Ku70/80, PARP-1, and topoisomerase IIβ, as well as protein phosphatase 1, are recruited to the fatty acid synthase promoter in mice immediately after feeding (Wong et al., 2009). Transient DNA breaks were recently reported to be required for estrogen-receptor-regulated transcription (Ju et al., 2006), and ATM is hypothesized to be required for the DNA-break-dependent transcriptional regulation of C/EBPα, similar to the case for DNA-PK. Indeed, topoisomerase β is phosphorylated in an ATM-dependent manner in response to DNA damage (Bensimon et al., 2010).

The amount of intrascapular and subcutaneous fat tissue in $Atm^{-/-}$ mice was less than that of their wild-type littermates. Conversely, $Atm^{-/-}$ mice showed an increased amount of visceral fat tissue, as previously reported (Schneider et al., 2006), comparable to that observed in lipodystrophy, HIV infection, or human metabolic syndrome, conditions that are associated with a high accumulation of visceral fat (Matsuzawa, 2006; Safrin and Grunfeld, 1999). Although it is not known why subcutaneous fat tissue is preferentially affected in $Atm^{-/-}$ mice, we propose several hypotheses to explain this phenomenon. First, the increased appetite of $Atm^{-/-}$ mice due to their reduced leptin level may preferentially induce fat accumulation in the visceral fat tissue (Figure S1O). Second, the caveolin-1 knockout mouse is one of the best-characterized lipodystrophic mouse models. Although this phenotype is observed late in life, all types of fat tissues in this mouse exhibit the lipodystrophic phenotype. As young animals, the only types of adipose tissue that are affected are the female mammary and subcutaneous white adipose tissue (Razani et al., 2002). As previously reported for caveolin-1 knockout mice, subcutaneous fat tissue of $Atm^{-/-}$ mice may be much more sensitive than other fat tissues to defects in the adipocyte differentiation machinery. Third, the association between age and lipodystrophy may be mediated by the increased number of deletions in the mitochondrial (mt) DNA that naturally occur with aging (Walker and Brinkman, 2001). Because visceral abdominal fat is known to be more metabolically active than other fat tissues, altered adipocyte mitochondrial functioning would affect central adipocytes more than peripheral adipocytes. It is known that ATM is indispensable for mitochondrial metabolism (Valentin-Vega et al., 2012). Based on these observations, one can speculate that loss of ATM would preferentially affect peripheral adipocytes, in which mitochondrial functioning is relatively low.

Our study revealed a previously uncharacterized function for ATM as a regulator of key adipocyte transcription factors, although its role in the DNA damage response pathway remains to be determined. Based on our findings, agents such as the PPARγ ligand thiazolidione, which induces adipocytic differentiation by bypassing the ATM pathway, may be good candidates for treating glucose intolerance in A-T patients.

It is interesting that in $Atm^{+/-}$ mice, a high-fat diet, but not a normal diet, induced glucose intolerance. Schneider et al. reported that $Atm^{+/-}ApoE^{-/-}$ mice fed a normal diet exhibited glucose intolerance (Schneider et al., 2006). However, in our study, $Atm^{+/-}$ mice did not exhibit glucose intolerance, although the genetic background of the $Atm^{+/-}ApoE^{-/-}$ mice or the increased serum lipid level generated by disabling the *ApoE* gene may have affected the state of glucose tolerance. Nevertheless, our observations demonstrated the possibility of an increased risk of metabolic syndrome in A-T carriers, which is consistent with the epidemiological data supporting an

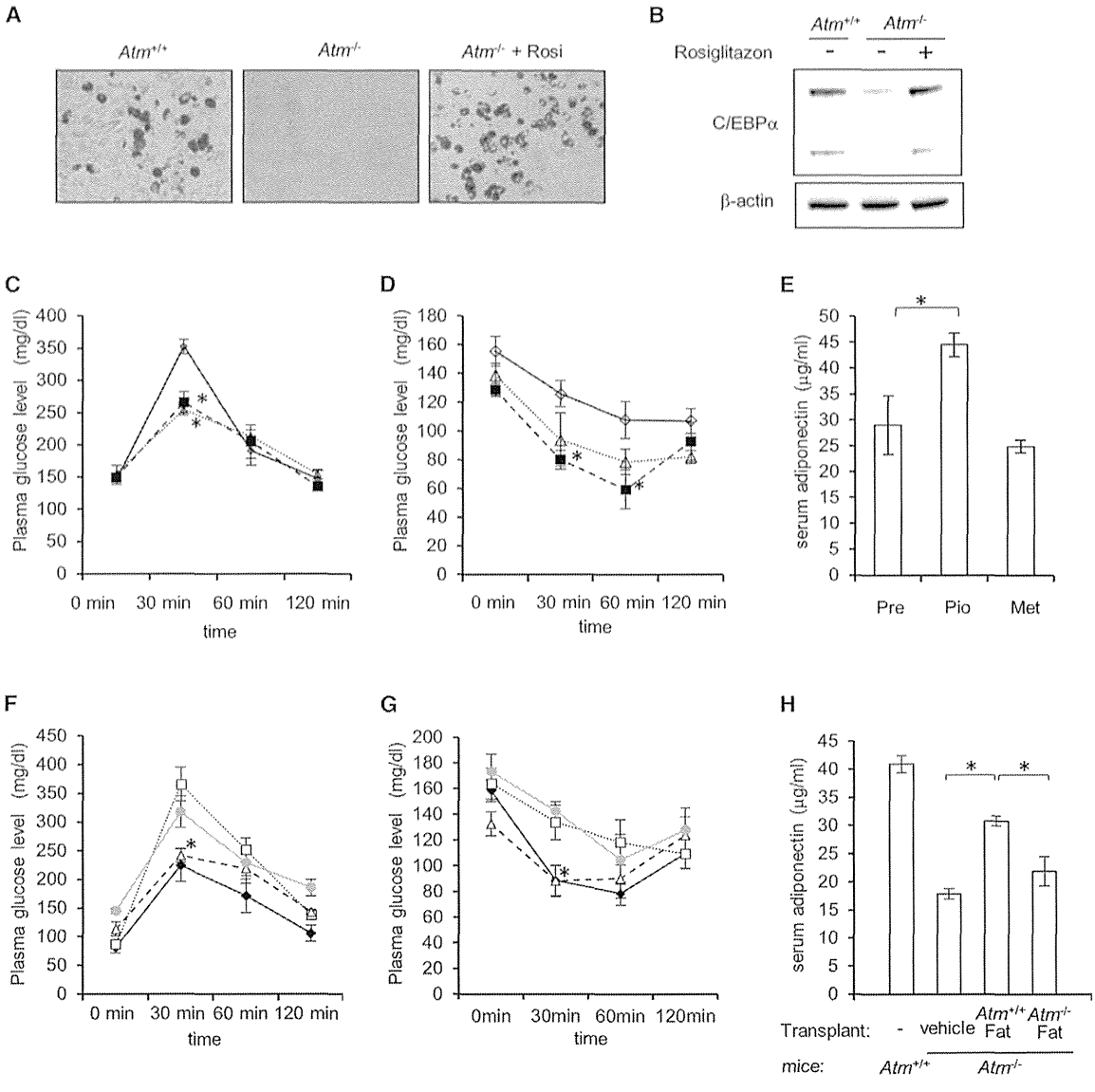

Figure 7. Thiazolidione Treatment and Wild-Type Adipose Tissue Transplantation Rescues the Glucose-Intolerance Phenotype of *Atm* Knockout Mice

(A) Rosiglitazone (Rosi) treatment restored the adipocyte differentiation capacity of $Atm^{-/-}$ MEFs. Oil red O staining (left).

(B) Western blotting analysis. Differentiation was induced using DMSO or 1 μM rosiglitazone.

(C) Results of glucose tolerance tests of $Atm^{-/-}$ mice treated with metformin or pisoglitazone. These tests were performed before treatment (open diamond), after metformin treatment (37.5 mg/kg, open triangle), and after pioglitazone treatment (30 mg/kg, closed square) for 21 consecutive days.

(D) Results of the insulin tolerance tests of mice treated as in (C).

(E) The serum adiponectin concentration of $Atm^{-/-}$ mice before treatment (Pre) with pioglitazone (Pio) or metformin (Met). The mean values from three or four independent experiments are shown.

(F) Results of the glucose tolerance tests performed after fat transplantation; $Atm^{+/+}$ mice (closed diamond), $Atm^{-/-}$ vehicle-transplanted mice (closed square), $Atm^{-/-}$ mice transplanted with $Atm^{+/+}$ fat (open triangle), and $Atm^{-/-}$ mice transplanted with $Atm^{-/-}$ fat (gray circle).

(G) Results of the insulin tolerance tests of mice treated as in (G).

(H) The serum adiponectin concentrations in $Atm^{+/+}$, $Atm^{-/-}$ vehicle-transplanted, and $Atm^{-/-}$ mice that received fat tissue transplants from $Atm^{+/+}$ mice or $Atm^{-/-}$ mice are shown in the bar graph. The mean values from three or four independent experiments are shown.

The SEs are shown as error bars (*$p < 0.05$).

increased risk for ischemic disease in A-T carriers (Su and Swift, 2000).

The *ATM* gene contains a number of SNPs, some of which confer functional deficiencies. The frequency of these SNPs is estimated to be <5%. One report demonstrated that a genetic locus responsible for type 2 diabetes is located on chromosome 11q, where *ATM* is also located (Palmer et al., 2006). A genome-wide association study showed that one SNP,

rs11212617, at the *ATM* locus was associated with the successful treatment of type 2 diabetes using metformin, suggesting that ATM plays a role in the effect of metformin upstream of AMPK (Zhou et al., 2011). Nucleotide variations or the inhibition of ATM using KU-55933 alters the glycemic response to metformin. However, the results of several studies do not support the hypothesis that ATM is involved in the activation of AMPK through metformin (Florez et al., 2012; Woods et al., 2012; Yee et al., 2012). Metformin activates the ATM-dependent pathway and inhibits tumor growth and the sensitivity to irradiation via an AMPK-dependent pathway (Storozhuk et al., 2013; Vazquez-Martin et al., 2011). However, further studies are required to elucidate the relationship between the metformin-dependent glycemic response and ATM-dependent glucose metabolism or the DNA damage response. It is also known that individuals with type 2 diabetes have an increased susceptibility to cancer. Together, these observations raised the question of whether *ATM* SNPs are associated with the concomitant susceptibility to diabetes and malignancy in certain individuals.

Thus, our study revealed a previously uncharacterized function for ATM in the regulation of key adipocyte transcription factors, although its role as a classical DNA damage response molecule remains to be determined. Understanding the functions of ATM that are modulated by the DNA damage response in glucose homeostasis may yield breakthroughs and reconsideration of the current paradigm for general diabetes research.

EXPERIMENTAL PROCEDURES

Animals

The generation of Atm-deficient mice ($Atm^{-/-}$) was previously described (Herzog et al., 1998). These mice have been backcrossed onto the C57BL/6 background for more than 15 generations. The mice were housed in a specific pathogen-free barrier facility and weaned at 3 weeks of age to a standard mouse chow that provided 6% of calories as fat. To produce the high-fat diet group, mice were fed a diet that provided 42% of calories as fat. Animal protocol 010018A was approved by the Animal Study Committee of Tokyo Medical and Dental University.

Glucose Tolerance Test, Insulin Sensitivity Assay, Surgical Implantation of Fat, and Pioglitazone and Metformin Treatment

$Atm^{-/-}$ mice fed normal chow underwent glucose tolerance or insulin resistance tests at 12 weeks of age. The mice were fasted for 12 hr, and then 10% D-glucose (1 g/kg body weight) or human insulin (0.75 U/kg body weight; Sigma-Aldrich) was administered via injection. Tail-vein blood (5 μl) was assayed for glucose at 0, 30, 60, and 120 min after the injection using a glucose meter (Medisense and Precision Xceed, Abbott Laboratories). Surgical implantation of fat was performed as previously reported, with minor modifications (Gavrilova et al., 2000). Intrascapular fat pads lacking brown adipose tissue and inguinal fat pads were used. The homeostasis model assessment (HOMA) index was calculated according to the following formula: insulin (μU/ml) × glucose (mg/dl)/405) (Akagiri et al., 2008). Pioglitazone and metformin were administered as previously described (Kita et al., 2012; Prieur et al., 2013).

Cells and Culture Conditions

3T3-L1 and 293T cells were maintained in DMEM supplemented with 10% fetal calf serum, 2 mM glutamine, and 100 U/ml of penicillin and streptomycin (P/S). Primary MEFs were cultured in medium supplemented with 0.1 mM nonessential amino acids, 55 μM 2-mercaptoethanol, and 100 U/ml P/S. The $Atm^{+/+}$ and $Atm^{-/-}$ MEF cell lines were maintained on an *Arf*-null background as described previously (Kamijo et al., 1999). In terms of adipocyte differentiation, the *Arf*-null background did not affect competency, similar to the case of the 3T3-L1 cell line, which lacks *Arf* expression.

In Vitro Adipocyte Differentiation Assay

The in vitro adipocyte differentiation assay was performed as previously described (Tanaka et al., 1997). To induce adipocytic differentiation, the cells were maintained at confluence for 2 days and were then switched to differentiation medium (DMEM containing 5 μg/ml insulin, 1 μM dexamethasone, and 0.5 mM isobutyl methyl xanthine [Sigma-Aldrich]). The medium was replaced every 2 days until the cells were analyzed. SVF analysis and in vitro differentiation were performed as previously described (Rodeheffer et al., 2008).

Oil Red O Staining and Determination of Triglyceride Content

To stain adipocytes, the cells were washed twice with PBS and then incubated with a filtered solution of 60% Oil red O (0.15 g/50 ml of 2-propanol) for 30 min at 37°C. The cells were washed briefly with 60% 2-propanol and then with water before visualization. To measure their triglyceride content, the cells were suspended in a buffer containing 150 mM NaCl, 10 mM Tris-HCl (pH 8.0), 0.1% Triton X-100, and protease inhibitors (Roche Diagnostics) and were sonicated for 10 s on ice. The lysates were cleared by centrifugation, and the triglyceride content was measured using a serum triglyceride determination kit (Sigma).

Western Blotting and Immunoprecipitation

Western blotting was performed according to routine procedures. The immunoprecipitation experiments were performed as follows. First, the cells were lysed using TGN buffer (50 mM Tris-HCl [pH 7.5], 150 mM NaCl, 1% NP-40, 0.5% Tween 20, and a phosphatase- and protease-inhibitor cocktail), and then the antigens were precipitated using the antibodies described above after precleaning the lysates using a control immunoglobulin G and protein A/G Sepharose beads (Santa Cruz Biotechnology). The precipitants were eluted by boiling the beads in SDS buffer after six thorough washes using TGN buffer containing 0.3 M LiCl. After SDS-PAGE, the blots were incubated with the various antibodies and were visualized using TrueBlot technology (eBioscience).

Immunofluorescence Microscopy

The cells were fixed using 4% paraformaldehyde at room temperature for 15 min, permeabilized using 0.5% Triton X-100/PBS at room temperature for 5 min, blocked using 10% FBS/PBS, and stained using primary antibodies diluted in PBS containing 2% BSA overnight at 4°C. The primary antibodies were detected using an Alexa-488-conjugated anti-mouse secondary antibody (Invitrogen). The nuclei were stained using Vectashield containing DAPI (Vector). Images were captured using an FV10i confocal microscope (Olympus).

ChIP Assay

The ChIP assays were performed as previously described, with minor modifications (Berkovich et al., 2008). Protein-G Dynabeads were used instead of protein-A agarose beads. The antibodies used for the ChIP assays included C/EBPβ (H7) from Santa Cruz Biotechnology and acetyl-histone H3 (06-599) and H4 (06-866) from EMD Millipore. The primers used for the expression analysis of the C/EBPα promoter were previously reported (Tang et al., 2004).

Luciferase Assay

The C/EBPα-promoter luciferase-reporter plasmid was constructed as previously described (Tang et al., 1997). The luciferase activity was determined using the dual-luciferase reporter assay system (Promega).

Real-Time qPCR Assay

After RNA extraction with TRIzol reagent (Life Technologies), cDNAs were synthesized using Superscript III (Life Technologies) and an oligo dT primer. PCR amplification was performed using SYBR GreenER (Life Technologies), and the amplified PCR product was monitored using a Bio-Rad MiniOption cycler.

Additional methods are provided in the Supplemental Experimental Procedures.

SUPPLEMENTAL INFORMATION

Supplemental Information includes Supplemental Experimental Procedures and seven figures and can be found with this article online at http://dx.doi.org/10.1016/j.celrep.2015.01.027.

AUTHOR CONTRIBUTIONS

M.T. designed and performed experiments, analyzed the data, and wrote the manuscript. H.U. performed majority of experiments and analyzed the data. R.N. performed complementation assay. M.S. performed glucose uptake assay, EMSA assay, and vector construction. S.K. and J.P performed microscopic analysis. N.I. performed micro CT analysis. S.K. (TMDU), S.K. (Juntendo University), Y.T., and Y.K performed hyperinsulinemic-euglycemic clamp experiments. T.S. supported experiment for differentiation assay using stromal vascular fractions. T.S. and A.Y. supervised the experiment performed by H.U. Y.O. and S.M. supervised the project and designed experiments.

ACKNOWLEDGMENTS

This study was supported by a Grant-in-Aid from the Ministry of Education, Science, and Culture (grant 11939625), the Ministry of Health, Labor, and Welfare (grant 26310401), the Uehara Foundation, the Sumitomo Foundation, Morinaga Hoshikai, the Takeda Science Foundation, the Suzuken Memorial Foundation, and the Boshi Hoken Kyokai Foundation. We thank Atsuko Nishikawa for technical assistance. The *Atm* knockout mouse was kindly provided by Dr. Peter McKinnon (St. Jude Children's Research Hospital, Memphis, TN). The $Atm^{+/+}$ and $Atm^{-/-}$ MEF cell lines were kindly provided by Dr. Charles Sherr (St. Jude Children's Research Hospital). We thank Hikari Taka and Tsutomu Fujimura (Juntendo University, Tokyo) for performing the LC-MS analysis. We thank Kevin Urayama (Tokyo Medical and Dental University) for critical reading of the manuscript.

Received: January 1, 2014
Revised: December 16, 2014
Accepted: January 9, 2015
Published: February 12, 2015

REFERENCES

Abella, A., Dubus, P., Malumbres, M., Rane, S.G., Kiyokawa, H., Sicard, A., Vignon, F., Langin, D., Barbacid, M., and Fajas, L. (2005). Cdk4 promotes adipogenesis through PPARgamma activation. Cell Metab. *2*, 239–249.

Akagiri, S., Naito, Y., Ichikawa, H., Mizushima, K., Takagi, T., Handa, O., Kokura, S., and Yoshikawa, T. (2008). A mouse model of metabolic syndrome; increase in visceral adipose tissue precedes the development of fatty liver and insulin resistance in high-fat diet-fed male KK/Ta mice. J. Clin. Biochem. Nutr. *42*, 150–157.

Armata, H.L., Golebiowski, D., Jung, D.Y., Ko, H.J., Kim, J.K., and Sluss, H.K. (2010). Requirement of the ATM/p53 tumor suppressor pathway for glucose homeostasis. Mol. Cell. Biol. *30*, 5787–5794.

Bakkenist, C.J., and Kastan, M.B. (2003). DNA damage activates ATM through intermolecular autophosphorylation and dimer dissociation. Nature *421*, 499–506.

Bar, R.S., Levis, W.R., Rechler, M.M., Harrison, L.C., Siebert, C., Podskalny, J., Roth, J., and Muggeo, M. (1978). Extreme insulin resistance in ataxia telangiectasia: defect in affinity of insulin receptors. N. Engl. J. Med. *298*, 1164–1171.

Bensimon, A., Schmidt, A., Ziv, Y., Elkon, R., Wang, S.Y., Chen, D.J., Aebersold, R., and Shiloh, Y. (2010). ATM-dependent and -independent dynamics of the nuclear phosphoproteome after DNA damage. Sci. Signal. *3*, rs3.

Berkovich, E., Monnat, R.J., Jr., and Kastan, M.B. (2008). Assessment of protein dynamics and DNA repair following generation of DNA double-strand breaks at defined genomic sites. Nat. Protoc. *3*, 915–922.

Blevins, L.S., Jr., and Gebhart, S.S. (1996). Insulin-resistant diabetes mellitus in a black woman with ataxia-telangiectasia. South. Med. J. *89*, 619–621.

Fajas, L., Landsberg, R.L., Huss-Garcia, Y., Sardet, C., Lees, J.A., and Auwerx, J. (2002). E2Fs regulate adipocyte differentiation. Dev. Cell *3*, 39–49.

Fernandes, N.D., Sun, Y., and Price, B.D. (2007). Activation of the kinase activity of ATM by retinoic acid is required for CREB-dependent differentiation of neuroblastoma cells. J. Biol. Chem. *282*, 16577–16584.

Florez, J.C., Jablonski, K.A., Taylor, A., Mather, K., Horton, E., White, N.H., Barrett-Connor, E., Knowler, W.C., Shuldiner, A.R., and Pollin, T.I.; Diabetes Prevention Program Research Group (2012). The C allele of ATM rs11212617 does not associate with metformin response in the Diabetes Prevention Program. Diabetes Care *35*, 1864–1867.

Gavrilova, O., Marcus-Samuels, B., Graham, D., Kim, J.K., Shulman, G.I., Castle, A.L., Vinson, C., Eckhaus, M., and Reitman, M.L. (2000). Surgical implantation of adipose tissue reverses diabetes in lipoatrophic mice. J. Clin. Invest. *105*, 271–278.

Herzog, K.H., Chong, M.J., Kapsetaki, M., Morgan, J.I., and McKinnon, P.J. (1998). Requirement for Atm in ionizing radiation-induced cell death in the developing central nervous system. Science *280*, 1089–1091.

Ito, K., Hirao, A., Arai, F., Matsuoka, S., Takubo, K., Hamaguchi, I., Nomiyama, K., Hosokawa, K., Sakurada, K., Nakagata, N., et al. (2004). Regulation of oxidative stress by ATM is required for self-renewal of haematopoietic stem cells. Nature *431*, 997–1002.

Iwahori, S., Yasui, Y., Kudoh, A., Sato, Y., Nakayama, S., Murata, T., Isomura, H., and Tsurumi, T. (2008). Identification of phosphorylation sites on transcription factor Sp1 in response to DNA damage and its accumulation at damaged sites. Cell. Signal. *20*, 1795–1803.

Jang, E.R., Choi, J.D., Jeong, G., and Lee, J.S. (2010). Phosphorylation of p300 by ATM controls the stability of NBS1. Biochem. Biophys. Res. Commun. *397*, 637–643.

Ju, B.G., Lunyak, V.V., Perissi, V., Garcia-Bassets, I., Rose, D.W., Glass, C.K., and Rosenfeld, M.G. (2006). A topoisomerase IIbeta-mediated dsDNA break required for regulated transcription. Science *312*, 1798–1802.

Kamijo, T., van de Kamp, E., Chong, M.J., Zindy, F., Diehl, J.A., Sherr, C.J., and McKinnon, P.J. (1999). Loss of the ARF tumor suppressor reverses premature replicative arrest but not radiation hypersensitivity arising from disabled atm function. Cancer Res. *59*, 2464–2469.

Kim, J., and Wong, P.K. (2009). Loss of ATM impairs proliferation of neural stem cells through oxidative stress-mediated p38 MAPK signaling. Stem Cells *27*, 1987–1998.

Kita, Y., Takamura, T., Misu, H., Ota, T., Kurita, S., Takeshita, Y., Uno, M., Matsuzawa-Nagata, N., Kato, K., Ando, H., et al. (2012). Metformin prevents and reverses inflammation in a non-diabetic mouse model of nonalcoholic steatohepatitis. PLoS ONE *7*, e43056.

Lin, W.C., Lin, F.T., and Nevins, J.R. (2001). Selective induction of E2F1 in response to DNA damage, mediated by ATM-dependent phosphorylation. Genes Dev. *15*, 1833–1844.

Matsuoka, S., Ballif, B.A., Smogorzewska, A., McDonald, E.R., 3rd, Hurov, K.E., Luo, J., Bakalarski, C.E., Zhao, Z., Solimini, N., Lerenthal, Y., et al. (2007). ATM and ATR substrate analysis reveals extensive protein networks responsive to DNA damage. Science *316*, 1160–1166.

Matsuzawa, Y. (2006). The metabolic syndrome and adipocytokines. FEBS Lett. *580*, 2917–2921.

McFarlin, D.E., Strober, W., and Waldmann, T.A. (1972). Ataxia-telangiectasia. Medicine (Baltimore) *51*, 281–314.

Miles, P.D., Treuner, K., Latronica, M., Olefsky, J.M., and Barlow, C. (2007). Impaired insulin secretion in a mouse model of ataxia telangiectasia. Am. J. Physiol. Endocrinol. Metab. *293*, E70–E74.

Minamino, T., Orimo, M., Shimizu, I., Kunieda, T., Yokoyama, M., Ito, T., Nojima, A., Nabetani, A., Oike, Y., Matsubara, H., et al. (2009). A crucial role for adipose tissue p53 in the regulation of insulin resistance. Nat. Med. *15*, 1082–1087.

Morio, T., Takahashi, N., Watanabe, F., Honda, F., Sato, M., Takagi, M., Imadome, K., Miyawaki, T., Delia, D., Nakamura, K., et al. (2009). Phenotypic variations between affected siblings with ataxia-telangiectasia: ataxia-telangiectasia in Japan. Int. J. Hematol. *90*, 455–462.

Morrell, D., Chase, C.L., Kupper, L.L., and Swift, M. (1986). Diabetes mellitus in ataxia-telangiectasia, Fanconi anemia, xeroderma pigmentosum, common variable immune deficiency, and severe combined immune deficiency families. Diabetes *35*, 143–147.

Palmer, N.D., Langefeld, C.D., Campbell, J.K., Williams, A.H., Saad, M., Norris, J.M., Haffner, S.M., Rotter, J.I., Wagenknecht, L.E., Bergman, R.N., et al. (2006). Genetic mapping of disposition index and acute insulin response loci on chromosome 11q. The Insulin Resistance Atherosclerosis Study (IRAS) Family Study. Diabetes *55*, 911–918.

Park, B.H., Qiang, L., and Farmer, S.R. (2004). Phosphorylation of C/EBPbeta at a consensus extracellular signal-regulated kinase/glycogen synthase kinase 3 site is required for the induction of adiponectin gene expression during the differentiation of mouse fibroblasts into adipocytes. Mol. Cell. Biol. *24*, 8671–8680.

Peretz, S., Jensen, R., Baserga, R., and Glazer, P.M. (2001). ATM-dependent expression of the insulin-like growth factor-I receptor in a pathway regulating radiation response. Proc. Natl. Acad. Sci. USA *98*, 1676–1681.

Prieur, X., Dollet, L., Takahashi, M., Nemani, M., Pillot, B., Le May, C., Mounier, C., Takigawa-Imamura, H., Zelenika, D., Matsuda, F., et al. (2013). Thiazolidinediones partially reverse the metabolic disturbances observed in Bscl2/seipin-deficient mice. Diabetologia *56*, 1813–1825.

Raman, M., Earnest, S., Zhang, K., Zhao, Y., and Cobb, M.H. (2007). TAO kinases mediate activation of p38 in response to DNA damage. EMBO J. *26*, 2005–2014.

Razani, B., Combs, T.P., Wang, X.B., Frank, P.G., Park, D.S., Russell, R.G., Li, M., Tang, B., Jelicks, L.A., Scherer, P.E., and Lisanti, M.P. (2002). Caveolin-1-deficient mice are lean, resistant to diet-induced obesity, and show hypertriglyceridemia with adipocyte abnormalities. J. Biol. Chem. *277*, 8635–8647.

Rodeheffer, M.S., Birsoy, K., and Friedman, J.M. (2008). Identification of white adipocyte progenitor cells in vivo. Cell *135*, 240–249.

Rosen, E.D., and Spiegelman, B.M. (2000). Molecular regulation of adipogenesis. Annu. Rev. Cell Dev. Biol. *16*, 145–171.

Rosen, E.D., and Spiegelman, B.M. (2006). Adipocytes as regulators of energy balance and glucose homeostasis. Nature *444*, 847–853.

Safrin, S., and Grunfeld, C. (1999). Fat distribution and metabolic changes in patients with HIV infection. AIDS *13*, 2493–2505.

Schalch, D.S., McFarlin, D.E., and Barlow, M.H. (1970). An unusual form of diabetes mellitus in ataxia telangiectasia. N. Engl. J. Med. *282*, 1396–1402.

Schneider, J.G., Finck, B.N., Ren, J., Standley, K.N., Takagi, M., Maclean, K.H., Bernal-Mizrachi, C., Muslin, A.J., Kastan, M.B., and Semenkovich, C.F. (2006). ATM-dependent suppression of stress signaling reduces vascular disease in metabolic syndrome. Cell Metab. *4*, 377–389.

Schubert, R., Reichenbach, J., and Zielen, S. (2005). Growth factor deficiency in patients with ataxia telangiectasia. Clin. Exp. Immunol. *140*, 517–519.

Schwartz, C., Beck, K., Mink, S., Schmolke, M., Budde, B., Wenning, D., and Klempnauer, K.H. (2003). Recruitment of p300 by C/EBPbeta triggers phosphorylation of p300 and modulates coactivator activity. EMBO J. *22*, 882–892.

Shahrabani-Gargir, L., Pandita, T.K., and Werner, H. (2004). Ataxia-telangiectasia mutated gene controls insulin-like growth factor I receptor gene expression in a deoxyribonucleic acid damage response pathway via mechanisms involving zinc-finger transcription factors Sp1 and WT1. Endocrinology *145*, 5679–5687.

Shi, Y., Venkataraman, S.L., Dodson, G.E., Mabb, A.M., LeBlanc, S., and Tibbetts, R.S. (2004). Direct regulation of CREB transcriptional activity by ATM in response to genotoxic stress. Proc. Natl. Acad. Sci. USA *101*, 5898–5903.

Storozhuk, Y., Hopmans, S.N., Sanli, T., Barron, C., Tsiani, E., Cutz, J.C., Pond, G., Wright, J., Singh, G., and Tsakiridis, T. (2013). Metformin inhibits growth and enhances radiation response of non-small cell lung cancer (NSCLC) through ATM and AMPK. Br. J. Cancer *108*, 2021–2032.

Su, Y., and Swift, M. (2000). Mortality rates among carriers of ataxia-telangiectasia mutant alleles. Ann. Intern. Med. *133*, 770–778.

Tanaka, T., Yoshida, N., Kishimoto, T., and Akira, S. (1997). Defective adipocyte differentiation in mice lacking the C/EBPbeta and/or C/EBPdelta gene. EMBO J. *16*, 7432–7443.

Tang, Q.Q., Jiang, M.S., and Lane, M.D. (1997). Repression of transcription mediated by dual elements in the CCAAT/enhancer binding protein alpha gene. Proc. Natl. Acad. Sci. USA *94*, 13571–13575.

Tang, D., Wu, D., Hirao, A., Lahti, J.M., Liu, L., Mazza, B., Kidd, V.J., Mak, T.W., and Ingram, A.J. (2002). ERK activation mediates cell cycle arrest and apoptosis after DNA damage independently of p53. J. Biol. Chem. *277*, 12710–12717.

Tang, Q.Q., Otto, T.C., and Lane, M.D. (2003). Mitotic clonal expansion: a synchronous process required for adipogenesis. Proc. Natl. Acad. Sci. USA *100*, 44–49.

Tang, Q.Q., Zhang, J.W., and Daniel Lane, M. (2004). Sequential gene promoter interactions by C/EBPbeta, C/EBPalpha, and PPARgamma during adipogenesis. Biochem. Biophys. Res. Commun. *318*, 213–218.

Valentin-Vega, Y.A., Maclean, K.H., Tait-Mulder, J., Milasta, S., Steeves, M., Dorsey, F.C., Cleveland, J.L., Green, D.R., and Kastan, M.B. (2012). Mitochondrial dysfunction in ataxia-telangiectasia. Blood *119*, 1490–1500.

Vazquez-Martin, A., Oliveras-Ferraros, C., Cufí, S., Martin-Castillo, B., and Menendez, J.A. (2011). Metformin activates an ataxia telangiectasia mutated (ATM)/Chk2-regulated DNA damage-like response. Cell Cycle *10*, 1499–1501.

Walker, U.A., and Brinkman, K. (2001). An argument for mitochondrial toxicity in highly active antiretroviral therapy-induced lipoatrophy. AIDS *15*, 1450–1452.

Wang, H., Larris, B., Peiris, T.H., Zhang, L., Le Lay, J., Gao, Y., and Greenbaum, L.E. (2007). C/EBPbeta activates E2F-regulated genes in vivo via recruitment of the coactivator CREB-binding protein/P300. J. Biol. Chem. *282*, 24679–24688.

Wong, R.H., Chang, I., Hudak, C.S., Hyun, S., Kwan, H.Y., and Sul, H.S. (2009). A role of DNA-PK for the metabolic gene regulation in response to insulin. Cell *136*, 1056–1072.

Woods, A., Leiper, J.M., and Carling, D. (2012). The role of ATM in response to metformin treatment and activation of AMPK. Nat. Genet. *44*, 360–361.

Yang, D.Q., and Kastan, M.B. (2000). Participation of ATM in insulin signalling through phosphorylation of eIF-4E-binding protein 1. Nat. Cell Biol. *2*, 893–898.

Yee, S.W., Chen, L., and Giacomini, K.M. (2012). The role of ATM in response to metformin treatment and activation of AMPK. Nat. Genet. *44*, 359–360.

Zhang, J.W., Klemm, D.J., Vinson, C., and Lane, M.D. (2004). Role of CREB in transcriptional regulation of CCAAT/enhancer-binding protein beta gene during adipogenesis. J. Biol. Chem. *279*, 4471–4478.

Zhou, K., Bellenguez, C., Spencer, C.C., Bennett, A.J., Coleman, R.L., Tavendale, R., Hawley, S.A., Donnelly, L.A., Schofield, C., Groves, C.J., et al.; GoDARTS and UKPDS Diabetes Pharmacogenetics Study Group; Wellcome Trust Case Control Consortium 2; MAGIC investigators (2011). Common variants near ATM are associated with glycemic response to metformin in type 2 diabetes. Nat. Genet. *43*, 117–120.

Hindawi Publishing Corporation
Mediators of Inflammation
Volume 2014, Article ID 564091, 8 pages
http://dx.doi.org/10.1155/2014/564091

Research Article

Changes in Cerebrospinal Fluid Biomarkers in Human Herpesvirus-6-Associated Acute Encephalopathy/Febrile Seizures

Naoyuki Tanuma,[1,2] Rie Miyata,[2] Keisuke Nakajima,[2] Akihisa Okumura,[3] Masaya Kubota,[4] Shin-ichiro Hamano,[5] and Masaharu Hayashi[2]

[1] *Department of Pediatrics, Tokyo Metropolitan Fuchu Medical Center for the Disabled, 2-9-2 Musashidai, Fuchu, Tokyo 183-8553, Japan*
[2] *Department of Brain Development and Neural Regeneration, Tokyo Metropolitan Institute of Medical Science, Tokyo 156-8506, Japan*
[3] *Department of Pediatrics, School of Medicine, Juntendo University, Tokyo 113-8421, Japan*
[4] *Department of Neurology, National Center for Child Health and Development, Tokyo 157-8535, Japan*
[5] *Division of Neurology, Saitama Children's Medical Center, Saitama 339-8551, Japan*

Correspondence should be addressed to Naoyuki Tanuma; naoyuki_tanuma@member.metro.tokyo.jp

Received 20 June 2014; Revised 2 September 2014; Accepted 3 September 2014; Published 11 September 2014

Academic Editor: Yung-Hsiang Chen

To determine the involvement of oxidative stress in the pathogenesis of acute encephalopathy associated with human herpesvirus-6 (HHV-6) infection, we measured the levels of oxidative stress markers 8-hydroxy-2′-deoxyguanosine (8-OHdG) and hexanoyl-lysine adduct (HEL), tau protein, and cytokines in cerebrospinal fluid (CSF) obtained from patients with HHV-6-associated acute encephalopathy (HHV-6 encephalopathy) ($n = 16$) and complex febrile seizures associated with HHV-6 (HHV-6 complex FS) ($n = 10$). We also examined changes in CSF-8OHdG and CSF-HEL levels in patients with HHV-6 encephalopathy before and after treatment with edaravone, a free radical scavenger. CSF-8-OHdG levels in HHV-6 encephalopathy and HHV-6 complex FS were significantly higher than in control subjects. In contrast, CSF-HEL levels showed no significant difference between groups. The levels of total tau protein in HHV-6 encephalopathy were significantly higher than in control subjects. In six patients with HHV-6 infection (5 encephalopathy and 1 febrile seizure), the CSF-8-OHdG levels of five patients decreased after edaravone treatment. Our results suggest that oxidative DNA damage is involved in acute encephalopathy associated with HHV-6 infection.

1. Introduction

Viral infection-associated acute encephalopathy/encephalitis is a serious complication with neurological sequelae. The main symptoms of the acute phase are impaired consciousness and convulsive status epilepticus with hyperpyrexia. Several subtypes of acute encephalopathy have been established based on clinical, radiologic, and laboratory findings. Acute encephalopathy with biphasic seizures and late reduced diffusion (AESD) is a new subtype characterized by a prolonged febrile seizure (FS) on day 1, which usually lasts longer than 30 min, as the initial neurological symptom [1, 2]. The initial seizures are followed by secondary seizures, most often a cluster of complex partial seizures on days 4–6. Magnetic resonance imaging (MRI) shows no acute abnormalities until day 1 or 2 but reveals reduced subcortical diffusion from day 3 onwards. Hoshino et al. reported that AESD was the most frequent syndrome in a nationwide survey on the epidemiology of acute encephalopathy in Japan and that human herpesvirus-6 (HHV-6) was the most common preceding pathogenic infection in AESD [3]. Recent studies demonstrated three potential major pathomechanisms of viral associated encephalopathy: metabolic error, cytokine storm, and excitotoxicity [4]. However, the exact pathogenesis remains unknown.

Oxidative stress originates from an imbalance between the production of reactive oxygen species (ROS) and, to a lesser extent, reactive nitrogen species (RNS), and the antioxidant capacities of cells and organs [5]. Recently,

oxidative stress was confirmed to play a role in adult-onset neurodegenerative diseases such as Alzheimer's disease, Parkinson's disease, and amyotrophic lateral sclerosis [6, 7]. We confirmed the involvement of oxidative neuronal damage in child-onset neurodegenerative diseases, such as subacute sclerosing panencephalitis [8], xeroderma pigmentosum [9], Cockayne syndrome [10], and spinal muscular atrophy [11].

In the present study, we measured the levels of oxidative stress markers (8-hydroxy-2′-deoxyguanosine: 8-OHdG and hexanoyl-lysine adduct: HEL), tau protein, and cytokines in cerebrospinal fluid (CSF) obtained from patients with HHV-6-associated encephalopathy and complex FS associated with HHV-6 infection.

2. Patients and Methods

2.1. Patients. We analyzed CSF obtained in the acute phase of inpatients with HHV-6-associated encephalopathy (HHV-6 encephalopathy) ($n = 16$) and complex FS associated with HHV-6 (HHV-6 complex FS) ($n = 10$) during the period from 2008 to 2010. Laboratory diagnoses of HHV-6 infection were based on a virus-specific polymerase chain reaction (PCR) assay or detection of virus-specific antibodies. Diagnosis of acute encephalopathy or complex FS was performed by the attending physician and later confirmed by examination of available clinicoradiological information. All cases of HHV-6-associated encephalopathy were diagnosed based on the clinical course and MRI findings. The complex FS group consisted of children who presented with fever and seizure but were later found to be free from acute neurological damage based on the clinical course, laboratory data, and brain imaging. Another 16 children (15 with fever but not central nervous system infection and 1 with hypoglycemia) were also enrolled as control subjects. Parent consent was obtained in all subjects in accordance with the Helsinki Declaration and all protocols were approved by the institutional ethics committee of the Tokyo Metropolitan Fuchu Medical Center for the Disabled.

2.2. Sample Collection and Measurement of CSF Biomarkers. CSF samples were obtained from each patient at any point during the disease and immediately stored at −80°C until they were analyzed. The amount of DNA oxidative stress marker, 8-hydroxy-2′-deoxyguanosine (8-OHdG), and the early stage lipid peroxidation marker, hexanoyl-lysine adduct (HEL), was examined using commercially available enzyme-linked immunosorbent assay (ELISA) kits (Japan Institute for the Aging, Shizuoka, Japan). Total tau protein was determined using sandwich ELISA (Invitrogen Corporation, Camarillo, CA). The levels of cytokines were evaluated by multiplex bead-based immunoassay (BioPlex 200 system) (Bio-Rad Laboratories, Inc., Hercules, CA). All assays were carried out according to the manufacturer's protocols. The detection limit for each ELISA kit was 0.06 ng/mL (8-OHdG), 2.6 ng/mL (HEL), and 15 pg/mL (total tau protein).

2.3. Edaravone Treatment. Edaravone (3-methyl-1-phenyl-2-pyrazolin-5-one) is a free radical scavenging drug that is clinically used in Japan for treatment of acute ischemic stroke [12, 13]. Several studies have shown that edaravone has preventive effects on brain injury following ischemia and reperfusion in patients with brain attack [14, 15]. Based on these observations, six patients with HHV-6 infection (5 patients with encephalopathy and 1 patient with complex FS) received free radical scavenger edaravone treatment in addition to conventional therapy for acute encephalopathy. A standard treatment protocol is edaravone 0.5 mg/kg every 12 hours (1 mg/kg daily) intravenously for 7–12 days. Parent consent was obtained in all patients before the treatment.

2.4. Statistical Analysis. Data were analyzed by GraphPad Prism version 5.0. Differences in oxidative stress markers, tau protein, and cytokine levels among each group were analyzed by one-way analysis of variance (ANOVA) and Dunn's multiple comparison test. Correlations between CSF-8OHdG and other biomarkers were evaluated using Spearman's rank correlation coefficient. We used Fisher's exact test to examine the relationship between increased levels of each biomarker and the presence or absence of neurological sequelae in HHV-6 encephalopathy. Comparisons of levels of CSF biomarkers before and after edaravone treatment were performed by paired t-test. A P value of less than 0.05 was considered statistically significant.

3. Results

3.1. Study Population and Clinical Features. The characteristics of the patients included in the study are summarized in Table 1. There were no significant differences of age among each group. Thirteen of 16 patients (81.3%) with HHV-6 encephalopathy were AESD, and only five patients (31.3%) recovered without sequelae from HHV-6 encephalopathy. In contrast, all patients with complex FS associated with HHV-6 infection were without neurological sequelae.

3.2. Oxidative DNA Damage and Lipid Peroxidation in HHV-6 Encephalopathy and Complex FS. The CSF-8-OHdG levels in HHV-6 encephalopathy (0.129 ± 0.07 ng/mL, mean ± SD, $P < 0.01$) and HHV-6 complex FS (0.116 ± 0.061 ng/mL, mean ± SD, $P < 0.05$) patients were significantly higher than in control subjects (0.063 ± 0.01 ng/mL, mean ± SD) (Figure 1(a)). CSF-HEL levels (mean ± SD) in HHV-6 encephalopathy, HHV-6 complex FS, and control subjects were 3.59 ± 1.87 nmol/L, 5.24 ± 3.63 nmol/L, and 3.62 ± 1.08 nmol/L, respectively. There were no significant differences in CSF-HEL levels between all groups (Figure 1(b)). These data are summarized in Table 2.

3.3. Total Tau Protein Levels in HHV-6 Encephalopathy and Complex FS. Total tau protein levels in HHV-6 encephalopathy patients ($n = 16$) (13,905.6 ± 14,201.1 pg/mL, mean ± SD) were significantly higher than in control subjects (609.0 ± 342.0 pg/mL, mean ± SD) ($P < 0.05$, Figure 2). However, there were no significant differences in CSF tau protein levels between the HHV-6 encephalopathy group and HHV-6 FS group (654.7 ± 213.7 pg/mL, mean ± SD). We then divided

Table 1: Clinical characteristics of HHV-6 encephalopathy and febrile seizure patients.

	HHV-6 encephalopathy	HHV-6 complex febrile seizures	Controls
Number of patients	16	10	16
Age (months)	15.1 ± 5.4	12.6 ± 3.9	11.1 ± 10.8
Sex ratio (M : F)	8 : 8	5 : 5	11 : 5
Sampling time (day of illness)	1–8	1	—
MRI abnormality	14/16	ND	ND
Outcome (without sequelae)	5/16	10/10	—

HHV: human herpesvirus; No.: number; ND: not done; M: male; F: female; MRI: magnetic resonance imaging.

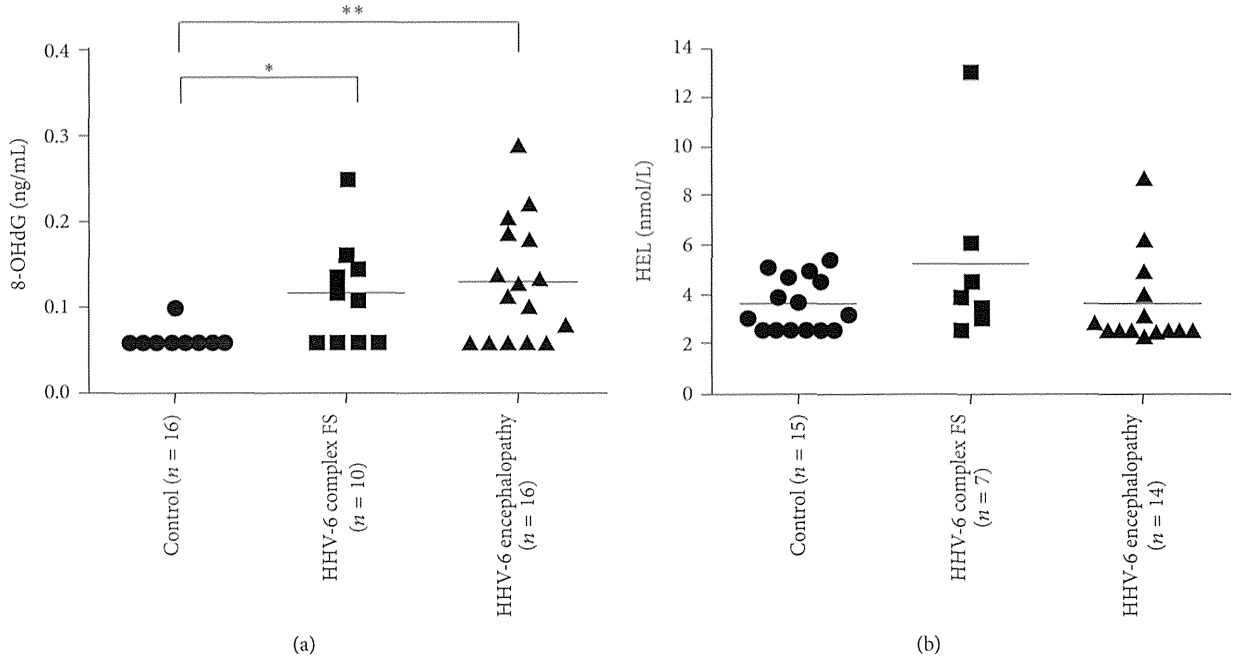

Figure 1: Cerebrospinal fluid (CSF) levels of oxidative stress markers in HHV-6 encephalopathy, HHV-6 complex febrile seizures (FS), and controls. (a) 8-hydroxy-2′-deoxyguanosine: 8-OHdG, (b) hexanoyl-lysine adduct: HEL. $^{*}P < 0.05$, $^{**}P < 0.01$. The horizontal bar indicates the mean value of each group. CSF-8OHdG levels (mean ± SD) in HHV-6 encephalopathy, HHV-6 complex FS, and controls are 0.129 ± 0.07 ng/mL, 0.116 ± 0.061 ng/mL, and 0.063 ± 0.01 ng/mL, respectively. CSF-HEL levels (mean ± SD) in HHV-6 encephalopathy, HHV-6 complex FS, and control subjects are 3.59 ± 1.87 nmol/L, 5.24 ± 3.63 nmol/L, and 3.62 ± 1.08 nmol/L, respectively.

Table 2: Descriptive statistics for the biomarkers examined[a].

Biomarkers	Controls	HHV-6 complex FS	HHV-6 encephalopathy	Global	*P*		
					Controls versus HHV-6 FS	Controls versus HHV-6 encephalopathy	HHV-6 FS versus HHV-6 encephalopathy
8-OHdG, ng/mL	0.063 (0.01)	0.116 (0.061)	0.129 (0.07)	0.0025	<0.05	<0.01	ns
HEL, nmol/L	3.62 (1.08)	5.24 (3.63)	3.59 (1.87)	0.1863	ns	ns	ns
Tau, pg/mL	609.0 (342.0)	654.7 (213.7)	13,905.6 (14,201.1)	0.0028	ns	<0.05	ns
IL-6, pg/mL	3.2 (3.0)	5.8 (5.3)	74.6 (116.9)	0.0349	ns	<0.01	ns
IL-10, pg/mL	0.4 (0.3)	0.6 (0.8)	1.4 (2.1)	0.1663	ns	ns	ns
TNF-α, pg/mL	0.1 (0.1)	0.3 (0.5)	3.4 (4.0)	0.0036	ns	<0.01	<0.05

8-OHdG: 8-hydroxy-2′-deoxyguanosine; HEL: hexanoyl-lysine adduct; HHV-6: human herpesvirus-6; FS: febrile seizure; ns: not significant; IL: interleukin; TNF: tumor necrosis factor.

[a]Values are expressed as the mean (standard deviation).

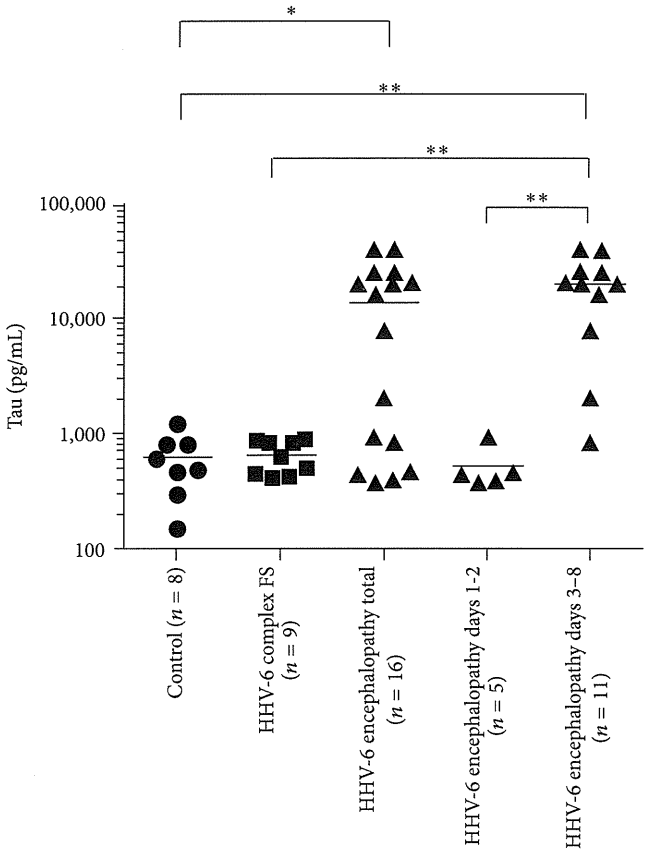

FIGURE 2: Cerebrospinal fluid (CSF) tau protein levels. The horizontal bar indicates the mean value of each group. CSF levels (mean ± SD) of tau protein in HHV-6 encephalopathy, HHV-6 complex febrile seizures (FS), and controls are 13,905.6 ± 14,201.1 pg/mL, 654.7±213.7 pg/mL, and 609.0±342.0 pg/mL, respectively. Total tau protein levels in HHV-6 encephalopathy patients are significantly higher than in control subjects ($^*P < 0.05$). The levels of tau protein in HHV-6 encephalopathy at days 3–8 (19,856.9 ± 13,121.9 pg/mL) are significantly higher than those of HHV-6 encephalopathy at days 1-2 (520.4 ± 229.6 pg/mL), HHV-6 complex FS, and controls ($^{**}P < 0.01$).

the HHV-6 encephalopathy group into two groups according to sampling time at days 1-2 ($n = 5$) and days 3–8 ($n = 11$), respectively. Consequently, we found that the levels of tau protein were significantly increased at days 3–8 in HHV-6 encephalopathy (19,856.9 ± 13,121.9 pg/mL, mean ± SD) compared with those of HHV-6 encephalopathy at days 1-2 (520.4 ± 229.6 pg/mL, mean ± SD) ($P < 0.01$), HHV-6 complex FS ($P < 0.01$), and controls ($P < 0.01$) (Figure 2).

3.4. CSF Cytokine Profile in Acute Encephalopathy and Complex FS. We next confirmed the elevation of CSF IL-6 and TNF-α in patients with HHV-6 encephalopathy (Figure 3). The CSF IL-6 levels in patients with HHV-6 encephalopathy (74.6 ± 116.9 pg/mL, mean ± SD) were significantly higher than in controls (3.2 ± 3.0 pg/mL, mean ± SD) ($P < 0.01$) (Figure 3(a)). The CSF TNF-α levels in patients with HHV-6 encephalopathy (3.4 ± 4.0 pg/mL, mean ± SD) were also significantly higher than those with complex FS (0.3 ± 0.5 pg/mL, mean ± SD) and in controls (0.10 ± 0.1 pg/mL, mean ± SD) ($P < 0.05$ and $P < 0.01$, resp.) (Figure 3(c)). In contrast, there were no significant differences of CSF IL-10 levels among patients with HHV-6 encephalopathy or HHV-6 complex FS and controls (Figure 3(b)).

3.5. Correlation Analysis of CSF Biomarkers in HHV-6 Encephalopathy. We next examined correlations between CSF-8OHdG and other biomarkers in the HHV-6 encephalopathy group (Table 3). There was a significant positive correlation between IL-6 and TNF-α (Spearman $r = 0.783$, $P = 0.0006$). However, there were no significant correlations among other biomarkers. In addition, there was no correlation between the increased levels of each biomarker and the presence or absence of neurological sequelae in HHV-6 encephalopathy (data not shown).

3.6. Changes in CSF-8-OHdG and CSF-HEL Levels before and after Edaravone Treatment in HHV-6-Associated Acute Encephalopathy and Complex FS. Finally, we compared the CSF levels of oxidative stress markers in six patients with HHV-6 infection (5 patients with encephalopathy and 1 patient with febrile seizures) before and after edaravone treatment. Clinical profile of patients with edaravone treatment is shown in Table 4. The mean initiation time of edaravone treatment was day 4.8 for the HHV-6 encephalopathy group. One patient with febrile seizures associated with HHV-6 infection who received edaravone treatment from day 1 did not develop encephalopathy and recovered without sequelae (patient 6). The CSF-8-OHdG levels decreased after edaravone treatment ($P = 0.0202$, paired t-test) (Figure 4(a)). Regarding the CSF-HEL levels, there were no significant differences between before and after edaravone treatment. We also compared the mean CSF levels of other biomarkers before and after treatment and observed no significant differences of mean values (data not shown).

4. Discussion

In the present study, we demonstrated that CSF-8-OHdG levels in HHV-6 encephalopathy and HHV-6 complex FS patients were significantly higher than in controls, suggesting increased oxidative stress is induced by HHV-6 infection. Recent studies revealed that oxidative damage is an emerging general mechanism of nervous system injury caused by viral infection. For example, oxidative injury is a component of acute encephalitis caused by herpes simplex virus type 1 (HSV-1) [16]. HSV-1 infection of nervous system tissues in mice was associated with the expression of inducible nitric oxide synthase (iNOS) and the release of cytokines including TNF-α from inflammatory cells. Thus, increased generation of ROS and RNS can be caused by the direct effects of virus on cells and the indirect effects of host inflammatory responses [17]. Regarding HHV-6 infection, Fukuda et al. reported that urinary 8-OHdG concentrations in a patient with HHV-6 encephalopathy on the first day of hospitalization were 1.5 times higher than the mean concentration

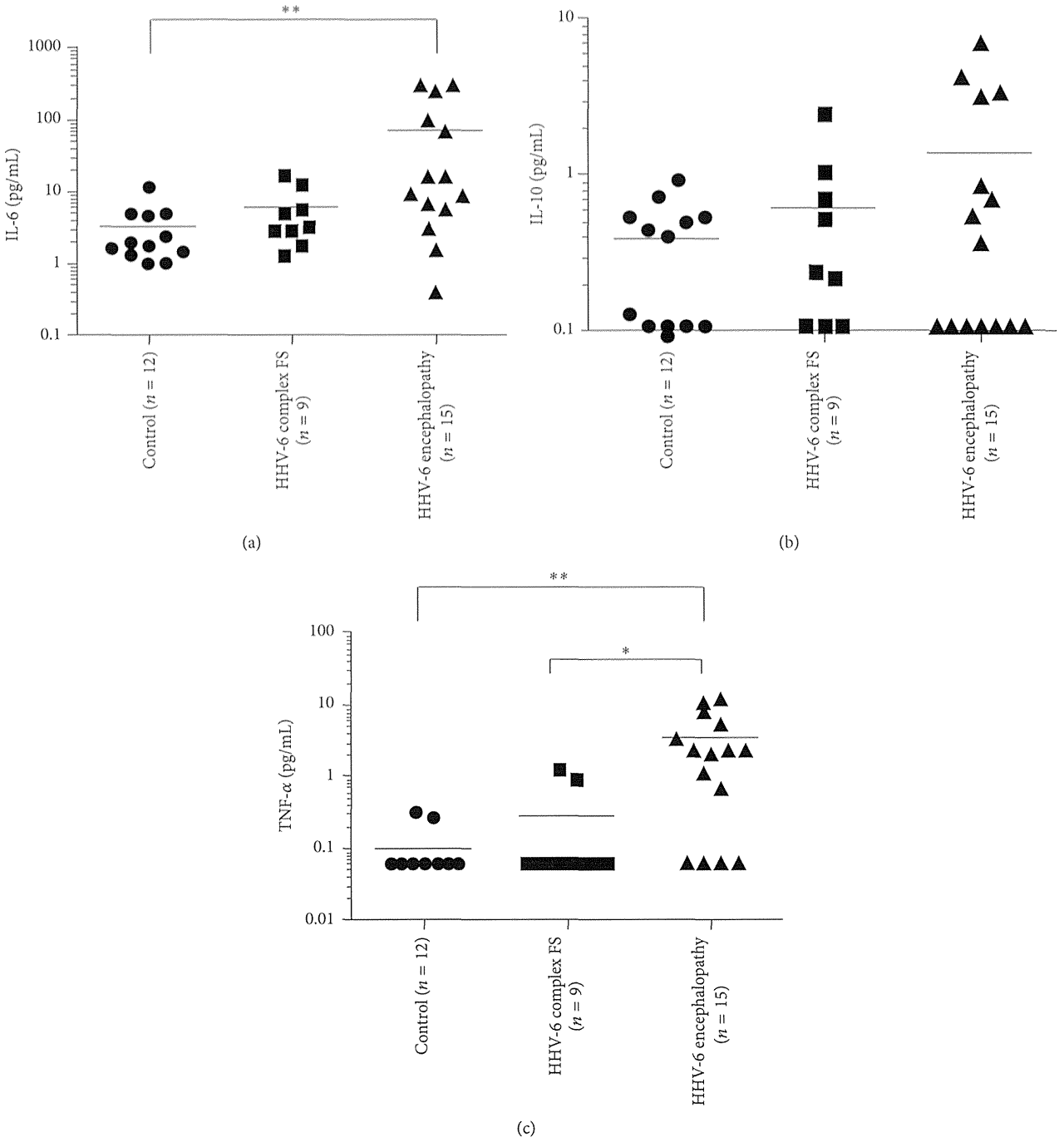

FIGURE 3: Cerebrospinal fluid (CSF) cytokine levels. The horizontal bar indicates the mean value of each group. (a) Levels of CSF IL-6 in patients with HHV-6 encephalopathy, HHV-6 febrile seizures (FS), and controls are 74.6 ± 116.9 pg/mL, 5.8 ± 5.3 pg/mL, and 3.2 ± 3.0 pg/mL, respectively. The CSF IL-6 levels in patients with HHV-6 encephalopathy are significantly higher than in controls ($^{**}P < 0.01$). (b) Levels of CSF IL-10 in patients with HHV-6 encephalopathy, HHV-6 febrile seizures (FS), and controls are 1.4 ± 2.1 pg/mL, 0.6 ± 0.8 pg/mL, and 0.4 ± 0.3 pg/mL, respectively. (c) Levels of CSF TNF-α in patients with HHV-6 encephalopathy, HHV-6 febrile seizures (FS), and controls are 3.4 ± 4.0 pg/mL, 0.3 ± 0.5 pg/mL, and 0.1 ± 0.1 pg/mL, respectively. The CSF TNF-α levels in patients with HHV-6 encephalopathy are significantly higher than those with complex FS and in controls ($^{*}P < 0.05$ and $^{**}P < 0.01$, resp.).

Table 3: Correlation analysis of CSF biomarkers in HHV-6 encephalopathy.

Biomarker		8-OHdG	HEL	Tau	IL-6	IL-10	TNF-α
8-OHdG	Spearman r	1.000	−0.292	−0.239	−0.484	−0.046	−0.315
	P	<0.0001	0.312	0.373	0.068	0.871	0.253
HEL	Spearman r	−0.292	1.000	0.277	0.476	−0.286	0.497
	P	0.312	<0.0001	0.338	0.086	0.322	0.070
Tau	Spearman r	−0.239	0.277	1.000	−0.036	−0.224	0.091
	P	0.373	0.338	<0.0001	0.899	0.422	0.748
IL-6	Spearman r	−0.484	0.476	−0.036	1.000	0.226	0.783
	P	0.068	0.086	0.899	<0.0001	0.418	0.0006
Il-10	Spearman r	−0.046	−0.286	−0.224	0.226	1.000	0.166
	P	0.871	0.322	0.422	0.418	<0.0001	0.555
TNF-α	Spearman r	−0.315	0.497	0.091	0.783	0.166	1.000
	P	0.253	0.070	0.748	0.0006	0.555	<0.0001

CSF: cerebrospinal fluid; HHV: human herpesvirus; 8-OHdG: 8-hydroxy-2′-deoxyguanosine; HEL: hexanoyl-lysine adduct; IL: interleukin; TNF: tumor necrosis factor.

Table 4: Clinical profile of patients receiving edaravone treatment.

Patient	Clinical diagnosis	Age/sex	Initiation and dosage of edaravone treatment	Other treatments	Outcomes
1	HHV-6 encephalopathy	14 m/M	Day 5 0.5 mg/kg × 2/day × 7 days	Mannitol, Dexamethasone, Ganciclovir, MDL, PHT	Intellectual disability
2	HHV-6 encephalopathy (AESD)	12 m/F	Day 5 0.5 mg/kg × 2/day × 8 days	Mannitol, Dexamethasone, Ganciclovir, DZP, MDL	Without sequelae
3	HHV-6 encephalopathy	14 m/M	Day 4 0.5 mg/kg × 2/day × 10 days	Mannitol, Dexamethasone, Ganciclovir/acyclovir, DZP, MDL	Hemophagocytic syndrome Died of fulminant hepatitis
4	HHV-6 encephalopathy (AESD)	20 m/F	Day 7 0.5 mg/kg × 2/day × 7 days	Mannitol, Dexamethasone, Aciclovir, MDL	Lt hemiparesis
5	HHV-6 encephalopathy (AESD)	12 m/M	Day 3 15 mg/day × 10 days	DZP, MDL, steroid pulse therapy, mild therapeutic hypothermia	Moderate psychomotor retardation
6	HHV-6 febrile seizures	10 m/F	Day 1 0.5 mg/kg × 2/day × 12 days	Mannitol, Dexamethasone, Ganciclovir/acyclovir, DZP, MDL, PHT	Without sequelae

m: months; M: male; F: female; DZP: diazepam; MDL: midazolam; PHT: phenytoin; Lt: left; HHV: human herpesvirus; AESD: acute encephalopathy with biphasic seizures and late reduced diffusion.

in healthy children and they peaked at the second seizures [18]. They speculated that 8-OHdG was produced by ROS from cytokines associated with inflammation and apoptosis following brain edema because changes in urinary 8-OHdG levels reflected the degree of brain edema. However, we found that increased levels of 8-OHdG were observed not only in HHV-6 encephalopathy but also in complex FS associated with HHV-6 infection. We also showed that CSF IL-6 and TNF-α levels were elevated only in the HHV-6 encephalopathy group, but not in the HHV-6 complex FS group. In addition, we analyzed correlations among biomarkers and observed no significant correlations between increased 8-OHdG levels and cytokine production or increased tau levels. These results suggest that oxidative DNA damage in the brain caused by HHV-6 infection may be independent of inflammatory reactions and subsequent axonal damage.

In contrast with the increased levels of 8-OHdG, there was no significant increase of CSF-HEL levels in HHV-6 encephalopathy compared with HHV-6 complex FS and controls. We previously demonstrated that oxidative stress

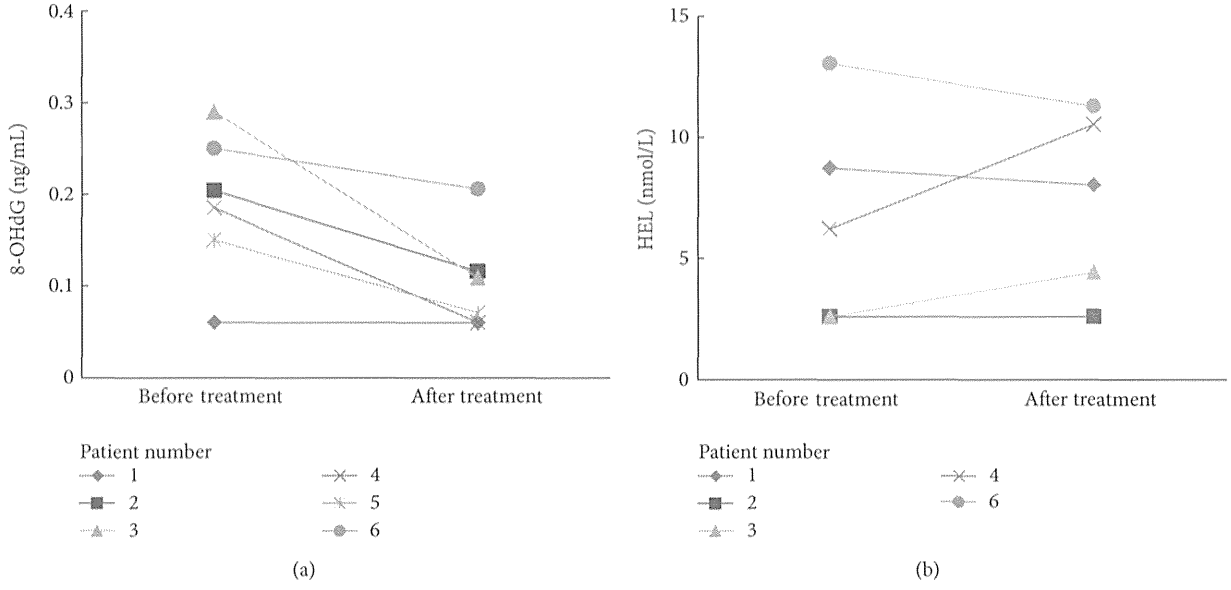

FIGURE 4: Changes in cerebrospinal fluid (CSF)-8-OHdG (a) and CSF-HEL (b) levels before and after edaravone treatment in HHV-6-associated acute encephalopathy and complex febrile seizure (FS) patients. CSF-8-OHdG levels are decreased after edaravone treatment ($P = 0.0202$, paired t-test).

of DNA contributes to early neuronal damage, whereas lipid peroxidation is related to subsequent neurodegeneration in subacute sclerosing panencephalitis [8]. In the present study, we only examined levels of CSF biomarkers in the acute phase of the diseases. Further investigation is required to clarify whether lipid peroxidation may be involved in the chronic phase.

Most patients with HHV-6 encephalopathy in this study (81.3%) were AESD, which has a high incidence of neurological sequelae. We previously indicated that levels of CSF tau protein were elevated in patients with AESD [19]. The current study demonstrates that CSF levels of tau protein were significantly increased at days 3–8 in HHV-6 encephalopathy compared with those of HHV-6 encephalopathy at days 1-2, HHV-6 complex FS, and controls. As CSF tau protein is considered a useful biomarker of axonal damage [20], our results raise the possibility that the high incidence of neurological sequelae in AESD is attributable to axonal injury. However, there was no correlation between the increased levels of tau protein and the presence or absence of neurological sequelae. These findings suggest that tau protein is a sensitive biomarker that might help diagnose HHV-6 encephalopathy, but it is difficult to make an early diagnosis for acute encephalopathy using this biomarker. In terms of the prognostic prediction for HHV-6 encephalopathy, another biomarker will be required because increased levels of tau protein do not always reflect a poor prognosis.

Edaravone is a free radical scavenger that interacts biochemically with a wide range of free radicals [21]. In experimental models, edaravone protects against apoptotic neuronal cell death and improves cerebral function after traumatic brain injury (TBI) [21]. In addition, Ohta et al. reported that administration of edaravone to mice immediately after TBI suppressed traumatic axonal injury and oxidative stress, which protected against trauma-induced memory deficits [22]. Edaravone is used clinically in Japan for the treatment of acute ischemic stroke. Although childhood ischemic stroke is different than in adults, the use of edaravone was recently approved for the treatment of stroke in children. In the present study, we reported 5 cases of edaravone treatment for HHV-6-associated acute encephalopathy and one case of HHV-6 complex FS. Our study is very preliminary and it is likely that the efficacy of edaravone treatment in combination with other therapies at this time was poor.

There were several limitations in this study. First, the initiation of edaravone treatment was delayed in HHV-6 encephalopathy because it is difficult to distinguish HHV-6 encephalopathy from HHV-6 complex FS during the initial seizures. Early diagnosis of HHV-6 encephalopathy, especially AESD, will be required to overcome this problem. Second, a clinical trial of edaravone for the treatment of acute encephalopathy might be difficult ethically, as placebo control cannot be used because of the severe nature of this disease. We confirmed that CSF-8-OHdG levels decreased after edaravone treatment, although there were no significant differences of mean values of other biomarkers between before and after the treatment. These results suggest edaravone treatment was partially effective for HHV-6 encephalopathy. Although these findings are encouraging, the therapeutic implications of ROS and RNS scavengers are complex, owing to their potential to exert toxic as well as protective effects [23].

5. Conclusion

In summary, we found oxidative DNA damage is involved in acute encephalopathy/febrile seizures associated with HHV-6 infection and may be independent of inflammatory reactions and subsequent axonal damage.

Conflict of Interests

The authors declare that there is no conflict of interests regarding the publication of this paper.

Acknowledgments

This study was supported by grants from the Ministry of Education, Culture, Sports, Science and Technology (22591147) and the Ministry of Health, Labour and Welfare (H23-Nanji-Ippan-107), Japan.

References

[1] J. Takanashi, H. Oba, A. J. Barkovich et al., "Diffusion MRI abnormalities after prolonged febrile seizures with encephalopathy," *Neurology*, vol. 66, no. 9, pp. 1304–1309, 2006.

[2] J.-I. Takanashi, "Two newly proposed infectious encephalitis/encephalopathy syndromes," *Brain and Development*, vol. 31, no. 7, pp. 521–528, 2009.

[3] A. Hoshino, M. Saitoh, A. Oka et al., "Epidemiology of acute encephalopathy in Japan, with emphasis on the association of viruses and syndromes," *Brain and Development*, vol. 34, no. 5, pp. 337–343, 2012.

[4] M. Mizuguchi, "Overview of acute encephalitis and encephalopathy," *Nippon Rinsho. Japanese Journal of Clinical Medicine*, vol. 69, no. 3, pp. 391–398, 2011.

[5] M. Hayashi, "Oxidative stress in developmental brain disorders," *Neuropathology*, vol. 29, no. 1, pp. 1–8, 2009.

[6] J. Emerit, M. Edeas, and F. Bricaire, "Neurodegenerative diseases and oxidative stress," *Biomedicine and Pharmacotherapy*, vol. 58, no. 1, pp. 39–46, 2004.

[7] K. Dasuri, L. Zhang, and J. N. Keller, "Oxidative stress, neurodegeneration, and the balance of protein degradation and protein synthesis," *Free Radical Biology and Medicine*, vol. 62, pp. 170–185, 2013.

[8] M. Hayashi, N. Arai, J. Satoh et al., "Neurodegenerative mechanisms in subacute sclerosing panencephalitis," *Journal of Child Neurology*, vol. 17, no. 10, pp. 725–730, 2002.

[9] M. Hayashi, M. Itoh, S. Araki et al., "Oxidative stress and disturbed glutamate transport in hereditary nucleotide repair disorders," *Journal of Neuropathology & Experimental Neurology*, vol. 60, no. 4, pp. 350–356, 2001.

[10] M. Hayashi, S. Araki, J. Kohyama, K. Shioda, and R. Fukatsu, "Oxidative nucleotide damage and superoxide dismutase expression in the brains of xeroderma pigmentosum group A and Cockayne syndrome," *Brain and Development*, vol. 27, no. 1, pp. 34–38, 2005.

[11] M. Hayashi, S. Araki, N. Arai et al., "Oxidative stress and disturbed glutamate transport in spinal muscular atrophy," *Brain and Development*, vol. 24, no. 8, pp. 770–775, 2002.

[12] E. Otomo, H. Tohgi, K. Kogure et al., "Effect of a novel free radical scavenger, edaravone (MCI-186), on acute brain infarction: Randomized, placebo-controlled, double-blind study at multicenters," *Cerebrovascular Diseases*, vol. 15, no. 3, pp. 222–229, 2003.

[13] B. J. Lee, Y. Egi, K. van Leyen, E. H. Lo, and K. Arai, "Edaravone, a free radical scavenger, protects components of the neurovascular unit against oxidative stress in vitro," *Brain Research*, vol. 1307, pp. 22–27, 2010.

[14] Y. Kitagawa, "Edaravone in acute ischemic stroke," *Internal Medicine*, vol. 45, no. 5, pp. 225–226, 2006.

[15] Y. Higashi, "Edaravone for the treatment of acute cerebral infarction: role of endothelium-derived nitric oxide and oxidative stress," *Expert Opinion on Pharmacotherapy*, vol. 10, no. 2, pp. 323–331, 2009.

[16] T. Valyi-Nagy and T. S. Dermody, "Role of oxidative damage in the pathogenesis of viral infections of the nervous system," *Histology and Histopathology*, vol. 20, no. 3, pp. 957–967, 2005.

[17] T. Akaike, "Role of free radicals in viral pathogenesis and mutation," *Reviews in Medical Virology*, vol. 11, no. 2, pp. 87–101, 2001.

[18] M. Fukuda, H. Yamauchi, H. Yamamoto et al., "The evaluation of oxidative DNA damage in children with brain damage using 8-hydroxydeoxyguanosine levels," *Brain & Development*, vol. 30, no. 2, pp. 131–136, 2008.

[19] N. Tanuma, R. Miyata, S. Kumada et al., "The axonal damage marker tau protein in the cerebrospinal fluid is increased in patients with acute encephalopathy with biphasic seizures and late reduced diffusion," *Brain and Development*, vol. 32, no. 6, pp. 435–439, 2010.

[20] M. Öst, K. Nylén, L. Csajbok et al., "Initial CSF total tau correlates with 1-year outcome in patients with traumatic brain injury," *Neurology*, vol. 67, no. 9, pp. 1600–1604, 2006.

[21] T. Itoh, T. Satou, S. Nishida et al., "Edaravone protects against apoptotic neuronal cell death and improves cerebral function after traumatic brain injury in rats," *Neurochemical Research*, vol. 35, no. 2, pp. 348–355, 2010.

[22] M. Ohta, Y. Higashi, T. Yawata et al., "Attenuation of axonal injury and oxidative stress by edaravone protects against cognitive impairments after traumatic brain injury," *Brain Research*, vol. 1490, pp. 184–192, 2013.

[23] T. Satoh and S. A. Lipton, "Redox regulation of neuronal survival mediated by electrophilic compounds," *Trends in Neurosciences*, vol. 30, no. 1, pp. 37–45, 2007.

RESEARCH LETTER

AMERICAN JOURNAL OF medical genetics PART A

Pathological Changes in Cardiac Muscle and Cerebellar Cortex in Vici Syndrome

Rie Miyata,[1] Masaharu Hayashi,[2]* and Eisaku Itoh[3]

[1]Department of Pediatrics, Tokyo Medical and Dental University, Tokyo, Japan

[2]Department of Brain Development and Neural Regeneration, Tokyo Metropolitan Institute of Medical Science, Tokyo, Japan

[3]Department of Pathology, Tokyo Medical and Dental University, Tokyo, Japan

Manuscript Received: 14 May 2014; Manuscript Accepted: 10 August 2014

TO THE EDITOR:

Vici syndrome [OMIM 242840] is a rare congenital disorder characterized by albinism, agenesis of corpus callosum, cardiomyopathy, and severe developmental and growth retardation [Vici et al., 1988; del Campo et al., 1999]. Neurological findings in Vici syndrome include hypotonia, seizures, nystagmus, and hypoplastic cerebellar vermis, in addition to agenesis of the corpus callosum [Miyata et al., 2007]. Recently, we identified recessive mutations in *EPG5* (previously *KIAA1632*) in patients with Vici syndrome [Cullup et al., 2013]. *EPG5* is the human homolog of metazoan-specific autophagy gene *epg-5*, encoding a key autophagy regulator (ectopic P-granules autophagy protein 5) implicated in the formation of autolysosomes. Autopsy on patients with Vici syndrome, including detailed neuropathologic findings, has rarely been reported [Rogers et al., 2011]. We examined the autopsy findings in the younger brother of siblings with Vici syndrome, in his sister *EPG5* mutations were confirmed.

He was born at term to nonconsanguineous parent, as previously reported [Miyata et al., 2007]. His sister was diagnosed with Vici syndrome clinically, and died at age one year. The *EPG-5* mutations were identified in fibroblasts, though autopsy was not granted by the parents [Cullup et al., 2013]. In the patient reported here, the combination of albinism, agenesis of corpus callosum, hypotonia, nystagmus, and severe developmental delay led to the diagnosis of Vici syndrome. He subsequently developed cardiomyopathy, epileptic seizures, and metabolic acidosis. Zonisamide was given from age 9 months. He died at 13 months when he suffered from gastroenteritis. The autopsy was granted by the parents.

The heart demonstrated dilation of the left ventricle. Histologically, there was neither severe degeneration nor fibrosis, but the mammillary muscles in the endocardium showed vacuole formation. We performed immunohistochemistry on autophagy in the heart, kidney and iliopsoas muscle in the patient and a 1-year-old control patient, who died of acute myelogenous leukemia and showed no pathological changes in the aforementioned organs. We used polyclonal antibody against microtubule-associated protein 1 light chain 3 (LC3), a well-known pathological marker of autophagy, in addition to monoclonal antibody against p62, a chief adapter protein in selective autophagy, which were purchased from Medical and Biological Laboratories, Nagoya, Japan. Cardiac muscle from the case and control were immunoreactive for LC3 uniformly, whereas lipofuscin in the cardiac muscle was immunoreactive for p62 only in the patient sample. The kidney and iliopsoas muscles had no changes in immunohistochemistry.

The brain (Fig. 1) was small, weighing 605 g. The cerebellum and brainstem were severely hypoplastic (A). The olfactory bulbs and optic chiasm were identified. On cross sections, the corpus callosum was absent completely, although Probst's bundles were not identified (B). The bilateral frontal operculum was hypoplastic. Histologically, the cerebral cortex in the frontal, parietal, temporal, and occipital cortex had formation of six layers (C), and neurons were spared in the cerebral cortex, the hippocampus (D) and the basal ganglia. The brainstem showed hypoplasia of the pyramidal tract (E). Other than the pyramidal tract, the transverse pontine fibers were reduced, suggesting the involvement of pontocerebellar fibers, possibly related to the hypoplastic cerebellum. In the cerebellar cortex, the Purkinje cells and granule cells were preserved comparatively well, although the formation of torpedo, axonal swelling of the Purkinje cells, was recognized in the inner granule layer throughout the cerebellum, including the vermis,

How to Cite this Article:
Miyata R, Hayashi M, Itoh E. 2014. Pathological changes in cardiac muscle and cerebellar cortex in vici syndrome.
Am J Med Genet Part A 164A:3203–3205.

Rie Miyata, Masaharu Hayashi, and Eisaku Itoh contributed equally to this work.

Conflict of interest: none.

*Correspondence to:
Masaharu Hayashi, Department of Brain Development and Neural Regeneration, Tokyo Metropolitan Institute of Medical Science, Tokyo, Japan.
E-mail: hayashi-ms@igakuken.or.jp

Article first published online in Wiley Online Library (wileyonlinelibrary.com): 24 September 2014
DOI 10.1002/ajmg.a.36753